



Norwegian University of
Science and Technology

Adaptive Vertical Motion Control System for a Surface Effect Ship

Snorre Ludvig Fjellvang

Marine Technology

Submission date: June 2018

Supervisor: Vahid Hassani, IMT

Co-supervisor: Øyvind Auestad, Umoe Mandal

Norwegian University of Science and Technology
Department of Marine Technology

Adaptive control of a Surface Effect Ship (SES)

A surface effect ship (SES) is a marine vehicle with a catamaran type hull and flexible rubber seals in the bow and stern end to enclose an air cushion that have high speed and superior sea-keeping performance in high seas compared to conventional catamarans [1]. SES is equipped with a lift system consisting of lift fans, and Vent Valves (VV) where the set of lift fans blow air into the air cushion with constant speed to pressurize it where the opening of the VV are controlled to generate desired lift which can carry close to 80% of the ships mass during transit. Also, the VV are actuators for vertical motions on a SES.

Umoe Mandal is currently the only shipyard in the world that launches SES. The shipyard has delivered several SES to the Norwegian Navy, such as the MTB Skjold class and the Mine Countermeasure Vessels (MCMV) series. Recently, the yard has focused on providing SES (WAVECRAFT) to the offshore wind industry.

Due to complex nature of SES, day-to-day operation of SES involves continuous manual adaptation of large number of tuning parameters. The operator must manually set certain control system parameters for the ventilation valve system (air out of the air cushion). The control parameter settings are highly affected by the environmental wave forces such as:

- Type of sea (long /short crested)
- Wave period
- Wave height
- Wave heading
- Vessel weight.

To illustrate the problem further, why not just set a high controller gain with high performance all of the time?

- In calm wave conditions, those high gains (that is excellent in high-seas) will produce vent valve servo instability since the process/measurement noise is amplified in a feedback loop.
- To reach the equilibrium (average cushion pressure) requirement, then by using high controller gains is equivalent to high airflow of the vent valves. Depending on the wind direction, this usually results in water spray on deck, which can make turbine technicians, wet. In rough seas, this is ok since safety is more important than a wet technician, but in low/medium seas, then this should be avoided, meaning lower gains are beneficial in such case.

Therefore, this master topic requests an adaptive control system where:

- The crew does not need to manually tune the controller gain
- The adaptive controller must adjust to varying sea conditions.
- The adaptive controller should not lead to unnecessary wear-and-tear on the vent valve assembly (hydraulic cylinder, hydraulic-electric servo-valve and mechanics), while still being able to damp motions in a satisfactory way.
- The system must be able to support damping of cg motions, bow tip motions and a combination of these two.
 - There are always equal, or more motion in the bow due to pitching, than CG. Therefore the gain must be adjusted accordingly for a good balance between motion damping performance and actuator wear-and-tear.

The proposed thesis includes modeling and developing control algorithms that can satisfy the requirements mentioned above. Currently simple, but effective, SES models exists, but

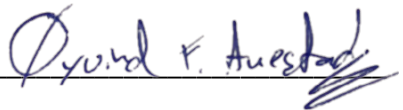
these needs to be further developed, verified and a new adaptive control system scheme must be designed.

The task will be supervised by

Adj. Associate professor Vahid Hassani from Department of Marine

Professor Jan Tommy Gravdahl from Department of Engineering Cybernetics

Technology, and Dr. Øyvind Auestad from Umoe Mandal.

A handwritten signature in blue ink, reading "Øyvind F. Auestad", written over a horizontal line.

Dr. Øyvind Auestad // Umoe Mandal

[1] Øyvind F. Auestad, (2015). The Boarding Control System. Ph.D. thesis, Norwegian University of Science and Technology.

Preface

This master thesis presents work done by marine cybernetics student Snorre Fjellvang at the Norwegian university of Science and Technology, NTNU. The thesis was completed between January and June 2018 with Adjunct Associate Professor Vahid Hassani as the main supervisor.

Work on the thesis was done in cooperation with UMOE Mandal with guidance from Dr. Øyvind Fidje Auestad. He has always been available to answer questions, and his knowledge on the Surface Effect Ship has been highly appreciated.

Trondheim, 2018-06-26

A handwritten signature in black ink, reading "Snorre Fjellvang". The signature is written in a cursive style with a long, sweeping flourish at the end.

Snorre Fjellvang

Executive Summary

In this thesis, an adaptive controller is developed, with the purpose of actuating the pressure of the air cushion of a Surface effect ship (SES), as means of reducing wave induced vertical vessel motions.

The rise in the offshore wind industry increases the demand for accessibility to wind turbines, which are located increasingly far off-shore. This sets new requirements for safety, with regards to both operations and maintenance. In general, the offshore wind industry is looking for new ways of utilizing the vessels characteristics to access turbines in rougher seas.

Control systems using actuation of the air cushion pressure to achieve active damping of vertical vessel motions are in existence today. However, operators are required to manually adjust the tuning parameters for the SES Motion Control System. By establishing a control system based on an adaptive control law, the crew members could be relieved of these tasks.

The basis for the control problem is that the controller parameters which provide the desired damping response, vary for the different operating conditions of the vessel. Changing environmental conditions and whether damping is desired directed towards the bow or the center of gravity, are factors contributing to why the current control system needs attention from the crew members. A poorly tuned controller may lead to wear on the actuators, cause vibrations or compromise the damping performance of the system. These are all aspects which have been taken into consideration in the design of the developed adaptive control system.

To test the adaptive controller, simulation models are used. These models are the results of decades of research and development of a mathematical description for the particular dynamics of the Surface Effect Ship. A simplified control plant model which incorporates the necessary vertical dynamics is implemented for the purpose of developing the controller. A more complex process plant model is supplied by UMOE Mandal and is used for verification purposes.

The controller is tested in simulations designed to emulate a range of different conditions which the vessel may encounter. Simulations are performed for regular and irregular sea states of varying amplitude and frequency, in addition to the application of control to both the bow and center of gravity of the vessel. The results show that the adaptive controller is able to achieve a desirable response in the range of the operating conditions tested.

Sammendrag

I denne oppgaven blir utviklingen av en adaptiv regulator beskrevet. Formålet med regulatoren er å justere trykket i luftputen på et Surface Effect Ship (SES), på en måte som reduserer bølgeinduserte vertikale bevegelser.

Fremgangen i offshore vindindustri øker etterspørselen etter vindturbiners tilgjengelighet. Samtidig blir vindturbinene plassert stadig lengre fra kysten. Dette stiller nye krav til sikkerhet, både med tanke på daglig drift og vedlikehold. Generelt er industrien til stadighet ute etter nye måter å utnytte de særegne egenskapene til SES på, for å kunne få adgang til vindturbiner i røffere sjøtilstander.

Kontrollsystemer som bruker aktivering av putetrykk for å oppnå aktiv demping av vertikale bevegelser er i drift idag. Derimot er mannskapet nødt til å gjøre manuelle justeringer på forsterkerparameterne i regulatoren for å oppnå ønsket ytelse fra systemet. Ved å introdusere et reguleringsystem basert på adaptiv kontroll, vil mannskapet kunne slippe disse oppgavene.

Grunnlaget for reguleringsproblemet er at de spesifikke parameterene som gir den ønskede dempingen, varierer avhengig av den operative tilstanden til fartøyet. Endringer i omgivelser og om en demping av bevegelser er ønsket i skipets baug eller massesenter er noen av aspektene som gjør at det nåværende reguleringsystemet regelmessig krever mannskapets oppmerksomhet. En dårlig justert regulator kan føre til unødvendig slitasje på aktuatorene, skape vibrasjoner eller svekke systemets evne til å dempe vertikale bevegelser. Dette er noen av faktorene som må tas til vurdering når den adaptive regulatoren skal utformes.

For å kartlegge ytelsen til den adaptive regulatoren blir simuleringsmodeller tatt i bruk. Disse modellene er resultatet av flere tiår med forskning på den matematiske beskrivelsen av dynamikken til et Surface Effect Ship. En forenklet modell, en såkalt *control plant*, som inkluderer den nødvendige dynamikken for å beskrive fartøyets vertikale bevegelser blir brukt for å utvikle regulatoren. En mer kompleks modell, en *process plant*, levert av UMOE Mandal blir brukt i verifikasjonsøyemed.

Regulatoren blir testet i ulike simuleringer, som er utformet for å etterligne de forskjellige forholdene fartøyet kan finne seg i. Simuleringene blir utført i regulære og uregulære sjøtilstander med varierende amplitude og frekvens, i tillegg til å endre punktet langs båten der dempingen blir påført fra baugen til massesenteret. Resultatene viser at den adaptive regulatoren er i stand til å fremkalle ønsket respons i de simulerte omgivelsene.

Contents

Preface	i
Executive Summary	ii
Sammendrag	iii
Nomenclature	vii
1 Introduction	3
1.1 Background	3
1.1.1 Motivation for Work	5
1.1.2 The Surface Effect Ship	5
1.1.3 Related Work	8
2 Mathematical Modeling	15
2.1 Coordinate Frame	15
2.2 Equation of Motion	16
2.3 Pressure Dynamics	17
2.4 Environment	20
2.5 SESSIM - Process Plant Model	22

2.6	Simplified Control Plant Model	24
2.6.1	Linear Pressure Model	24
2.6.2	State Space Model	25
2.6.3	Stability Investigation	26
3	Adaptive Vertical Motion Control	27
3.1	Feedback Controller	28
3.2	Parameter Adaptation	30
3.3	Controller Reference	31
3.4	Signal Processing	34
4	Results	35
4.1	Overview of Simulations	36
4.2	CPM Response in Regular Waves and Changing Sea State	36
4.2.1	Initialization and Transition from Hs 1.4 to 2 m	37
4.2.2	Initialization and Transition from Hs 2 to 1.4 m	39
4.3	CPM Response in Irregular Waves and Changing Sea State	41
4.3.1	Initialization and Transition from Hs 1 to 1.5 m	42
4.3.2	Initialization and Transition from Hs 1.5 to 1 m	44
4.4	SESSim Response in Irregular Waves	46
4.4.1	Initialization at Hs 1 m	47
4.4.2	Initialization at Hs 1.5 m	49
4.5	Response in Regular Waves - COG and Bow Damping	51
4.5.1	Initialization and Transition from COG to Bow Damping	52

4.5.2 Initialization and Transition from Bow to COG Damping	54
4.6 Discussions	56
5 Concluding remarks	58
5.1 Conclusion	58
5.2 Further Work	59
A Control Plant Model	61
A.1 Model Parameters	61
A.2 Controller parameters	62
B Additional results	63
B.1 CPM - Initialization and Transition from Hs 0.8 to 1.4 m - Regular Waves	64
B.2 CPM - Initialization and Transition from Hs 1.4 to 0.8 m - Regular Waves	65
C List of Attached Files	66
Bibliography	67

Nomenclature

Abbreviations

Abbreviation	Meaning
SES	Surface Effect Ship
ACV	Air Cushion Vehicle
CPM	Control Plant Model
RCS	Ride Control System
PPM	Process Plant Model
IMU	Inertial Measurement Unit
RAO	Response Amplitude Operator
BCS	Boarding Control System
LTI	Linear Time Invariant
COG	Center of Gravity
CTV	Crew Transfer Vessel
PSD	Power Spectral Density

List of Symbols

Variable	Definition
$A_L(t)$	Air cushion leakage area
H_s	Significant wave-height
$Q_{in}(t)$	Volumetric flow of air into the air cushion
$Q_{out}(t)$	Volumetric flow of air out of the air cushion
$\rho_c(t)$	Density of air inside the cushion
$V_c(t)$	Air cushion volume
L	Length of vessel
C_n	Orifice coefficient
$P_u(t)$	Uniform dynamic cushion pressure
P_0	Cushion equilibrium pressure
$V_0(t)$	Wave volume pumping
γ	Specific heat ratio of air
P_0	Cushion equilibrium pressure
$A_c(t)$	Cushion area
$x_{cp}(t)$	Distance between longitudinal COG and cushion center of pressure
V_{c0}	Equilibrium cushion volume
ω_p	Peak frequency of wave spectrum
$\zeta_a(t)$	Wave elevation
A_0	Mean operating cushion leakage area
$\mu_u(t)$	Non-dimensional dynamic cushion pressure
ρ_a	Ambient air density
h_0	Cushion height
Q_0	Equilibrium cushion air flow rate
$\theta(t)$	Feedback controller gain
ω_f	Butterworth filter cut-off frequency
$\Delta A_L(t)$	Change in cushion leakage area
V	Wind Speed
$\omega_e(t)$	Frequency of wave encounter

List of Figures

1.1	Cumulative and annual offshore wind energy installations (windeurope (2017)) . . .	4
1.2	Typical modern SES configuration (Courtesy of UMOE Mandal)	6
1.3	Left: Stern bag configuration, Right: Individual fingers making up the bow skirt . .	7
1.4	SES cross section displaying water level inside and outside of the hull	7
1.5	Heave Estimation Scheme (Auestad et al. (2013a))	12
1.6	Modeling of turbine contact (Auestad et al. (2015))	13
2.1	<i>Coordinate system definition</i>	16
2.2	<i>Control volume boundaries for the air cushion</i>	18
2.3	<i>Lift fan pump-curve</i>	19
2.4	<i>Realization of Jonswap spectra</i>	21
2.5	<i>Left: Wave-series with equally spaced frequencies and repeating structure, Right: Wave-series with noise added to the selection of frequencies</i>	22
3.1	<i>Basic overview of the adaptive control system</i>	27
3.2	<i>Vertical velocity development with $k_b = 0$ and $k_c = 1$ - COG damping - Initiation at 100s</i>	29
3.3	<i>Vertical velocity development with $k_b = 1$ and $k_c = 0$ - Bow damping - Initiation at 100s</i>	29

3.4	<i>Cost function development during control activation (400 s), transition to a higher sea state (1000-1200 s) and deactivation (1700 s)</i>	32
3.5	<i>Reference and measurement signal during initialization (Left) and transition to a higher sea state (Right)</i>	33
3.6	<i>Gain development during initialization, transition to a higher sea state and deactivation</i>	33
4.1	Simulation results for $H_s = 1.4\text{ m}$, $T_s = 7.5\text{ s}$ to $H_s = 2\text{ m}$, $T_s = 8.8\text{ s}$	37
4.2	Cost function value for varying feedback gain at $H_s = 1.4\text{ m}$, $T_s = 7.5\text{ s}$	38
4.3	Simulation results for $H_s = 2\text{ m}$, $T_s = 8.8\text{ s}$ to $H_s = 1.4\text{ m}$, $T_s = 7.5\text{ s}$	39
4.4	Cost function value for varying feedback gain at $H_s = 2\text{ m}$, $T_s = 8.8\text{ s}$	40
4.5	Jonswap wave spectra for $H_s = 1.5\text{ m}$ and $H_s = 1\text{ m}$ used in control plant model . .	41
4.6	Simulation results for $H_s = 1\text{ m}$, $\omega_p = 0.9\frac{\text{rad}}{\text{s}}$ to $H_s = 1.5\text{ m}$, $\omega_p = 0.8\frac{\text{rad}}{\text{s}}$	42
4.7	Power spectral density plot for $H_s = 1\text{ m}$ - Control Plant Model	43
4.8	Simulation results for $H_s = 1.5\text{ m}$, $\omega_p = 0.8\frac{\text{rad}}{\text{s}}$ to $H_s = 1\text{ m}$, $\omega_p = 0.9\frac{\text{rad}}{\text{s}}$	44
4.9	Power spectral density plot for $H_s = 1.5\text{ m}$ - Control Plant Model	45
4.10	Jonswap wave spectra for $H_s = 1.5\text{ m}$ and $H_s = 1\text{ m}$ used in SESSim model	46
4.11	Simulation results for $H_s = 1\text{ m}$, $\omega_p = 0.9\frac{\text{rad}}{\text{s}}$	47
4.12	Power spectral density plot for $H_s = 1\text{ m}$ - SESSim model	48
4.13	Simulation results for $H_s = 1.5\text{ m}$, $\omega_p = 0.8\frac{\text{rad}}{\text{s}}$	49
4.14	Power spectral density plot for $H_s = 1.5\text{ m}$ - SESSim model	50
4.15	Simulation results for $H_s = 1.5\text{ m}$, $T_s = 6\text{ s}$ - COG to Bow Damping	52
4.16	Simulation results for $H_s = 1.5\text{ m}$, $T_s = 6\text{ s}$ - Bow to COG Damping	54
B.1	Simulation results for $H_s = 1.4\text{ m}$, $T_s = 7.5\text{ s}$ to $H_s = 2\text{ m}$, $T_s = 8.8\text{ s}$	64

B.2 Simulation results for $H_s = 1.4 m$, $T_s = 7.5 s$ to $H_s = 2 m$, $T_s = 8.8 s$ 65

Chapter 1

Introduction

1.1 Background

First developed in the 1960s, the Surface Effect Ship (SES) is a unique type of vessel combining a catamaran hull and an encapsulated air cushion. This structure forms a vessel capable of reaching high speeds, while the surface piercing nature of the SES hull enables the usage of submerged water propulsion systems as opposed to an air cushion vehicle (ACV).

Historically, the development of the modern Surface Effect Ship took place with the intention of reaching increasingly higher speeds, which was anticipated to be of a huge impact in military applications (Butler (1985)). The idea behind the SES was that the air cushion, despite requiring a vast power input to sustain pressure, would support such a large portion of the weight of the vessel reducing the draft, and thereby the resistance. The power required to pressurize the air cushion is typically about 15% of the main engine power. Still, compared to a traditional mono-hull structure, the decrease in resistance is great enough to justify the energy input to the air cushion.

The development of the modern SES started as a military project. Over a couple of decades, several prototypes were launched and dozens of universities and contractors were involved. All leading up to a 3000 ton U.S. Navy SES that had a target speed of 80 knots. Unfortunately, the 3000 ton SES project was terminated in 1979 and the U.S. Navy stopped the SES development (Butler (1985)).

The SES had its commercial breakthrough in the 80s where the UK, US, USSR, China, France, Korea, Sweden and Norway were building SES Ferrys. For instance, the Norwegian shipyards

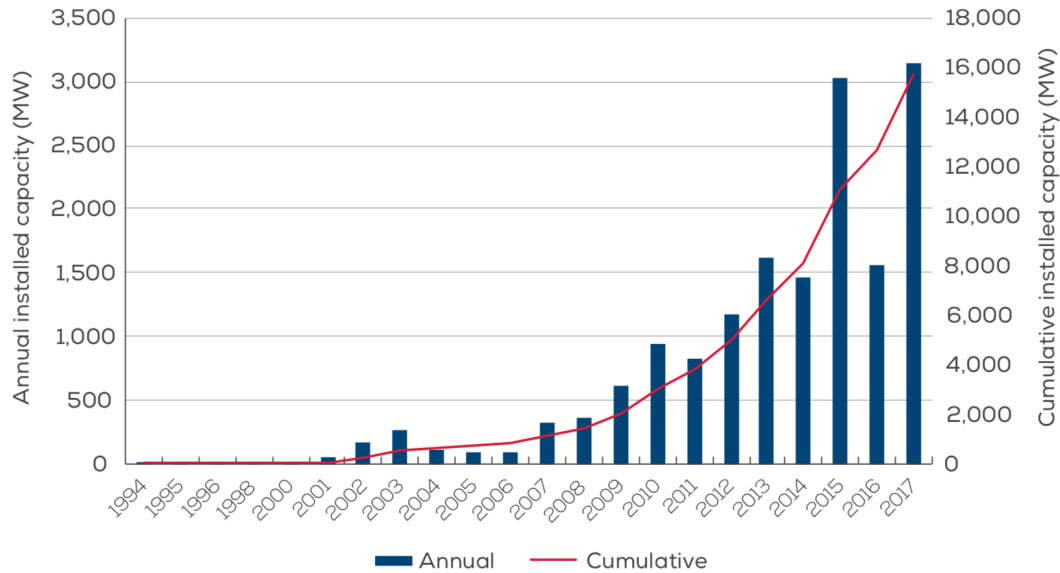


Figure 1.1: Cumulative and annual offshore wind energy installations (windeurope (2017))

Brødrene Aa, Westamarine and Ulstein built a total of 19 SES ferry's, with two or three of them still operating today.

Today, UMOE Mandal, located in Mandal, Norway, is at the forefront of research and development with regards to SES technology. Advancements in materials, engineering methods and technology feeds the progress in using the unique characteristics of the SES to establish a viable option for a high speed vessel with a low environmental impact.

Since the 1990s, UMOE Mandal have delivered several classes of vessels to the Norwegian Navy. In recent years, the focus has been on the development of the WAVECRAFT™ Crew Transfer Vessel for use in offshore oil and gas, renewables, passenger and defense purposes.

A major market for the WAVECRAFT™, is the offshore wind industry. Figure 1.1 depicts the development of wind turbine capacity in recent years in Europe alone. This trend, along with the fact that newly established wind farms average a distance from shore of 41 km, raises the demand for means of transporting crew and equipment between turbines (windeurope (2017)). As the distance from shore increases and the fact that wind farms in nature are required to be situated in locations prone to wind, and thus rough seas, crew accessibility for operation and maintenance purposes is limited.

To access the wind turbines, the crew are required to board the turbines from the transfer vessel. However, at higher seas, the relative motion between the turbine and vessel pose a safety issue during the boarding procedure. Dealing with this issue, UMOE Mandal has implemented

a Boarding Control System (BCS) (Auestad et al. (2015)) which by altering the pressure in the air cushion of the SES, in combination with the friction force between the turbine and vessel bow, is able to counteract a large portion of the wave induced vessel forces. A reduction in relative vertical motion between the vessel and turbine means a widening of the operational window of the turbine, which in turn contributed to less turbine downtime and an increase of annual energy production.

1.1.1 Motivation for Work

Today, the Boarding Control System (BCS) is in operation as a fundamental feature of the full-scale SES WAVECRAFT™ series. However, the current implementation introduces a set of tuning parameters for the control system, which have to be manually adjusted by the crew operators in order to obtain the desired performance at different sea states. If the control parameters are set too aggressive, this may lead to the actuators jumping between their upper and lower limits, which would cause unnecessary wear on the actuators. Moreover, if the control parameters are set too low the damping performance is limited.

The main goal of this thesis is investigating the possibilities of applying adaptive control theory to the existing control system, with the purpose of establishing a system where the BCS is able to function without the manual adjustments required of the operator today. This will result in a reduced workload for the crew and with more suitable chosen parameters for the control system. It is expected that the day-to-day average performance will increase considerably.

Following Auestad et al. (2015), a mathematical description of a simplified *control plant model* (CPM) is found. This description sets the foundation for the control system design used for testing of the developed adaptive scheme. Extending the scope of the existing model, is the implementation of irregular waves and a time-varying sea-state, which is required to test the adaptation capabilities of the controller.

1.1.2 The Surface Effect Ship

Surface Effect Ships are vessels with a catamaran type hull, with an enclosed air cushion between the two rigid side-hulls. In the longitudinal direction, the air inside the cushion is isolated by *bow-* and *stern-seals* (Figure 1.2), typically made of a flexible, elastic rubber-like material.

There are different approaches to the design of a SES depending on size, means of propulsion,

lift-capabilities and so on. The following section provides an overview of typical SES-specific characteristics, as described in Faltinsen (2005). These characteristics also fit the description of the WAVECRAFT™.

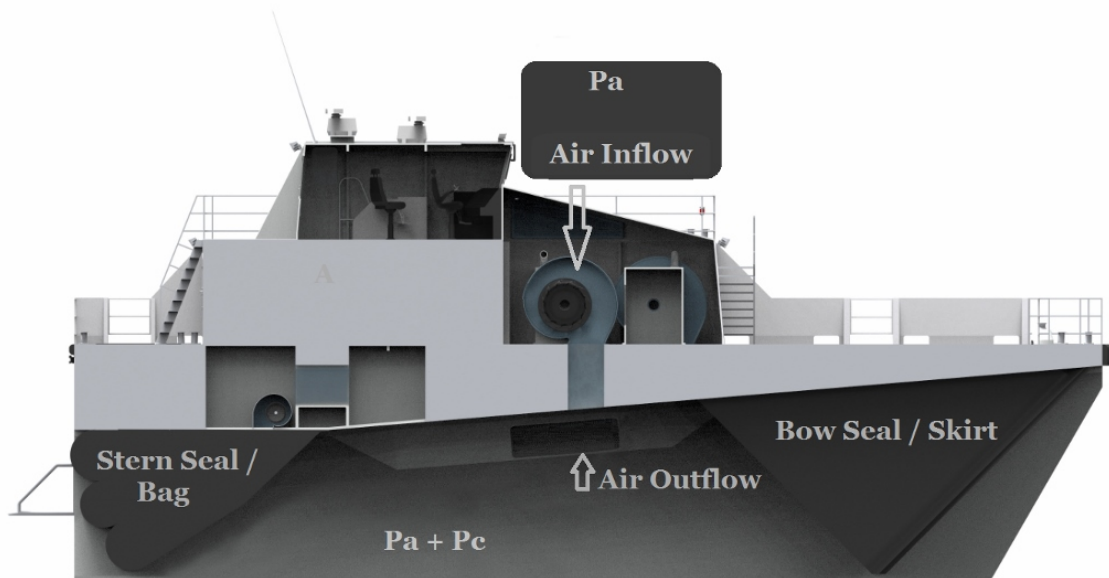


Figure 1.2: Typical modern SES configuration (Courtesy of UMOE Mandal)

The stern seal (Figure 1.3) is usually a bag made up of two or three loops of the rubber material stacked horizontally, with perforations in-between each loop to ensure equal pressure throughout the bag. The bow seal, often called the *skirt*, consists of several loops of rubber material in a side-by-side configuration. The stern bag holds a greater pressure than the main air cushion, to ensure sufficient sealing from the environment and reduce air leakage. This pressure is supplied by a *booster-fan*, configured to maintain a pressure level 5-15 % above that of the main cushion.

As part of the stern-bag design, there is a minor gap between the lowest lobe of the bag and the sea-surface at calm seas which contributes to some air-leakage from the air cushion. However, the gap allows the stern bag to have no water resistance at calm seas. Inflation of the skirt in the bow of the vessel comes from the excess pressure of the air cushion itself. There are sources of cushion air-leakage along both the stern and bow seals. However, this leakage is in all conditions a lot smaller than the flow of air through the main ventilation valves.

Supplying the excess pressure in the enclosed air cushion is an air-fan system, which consists of one or more *lift-fans*. These fans increase the pressure inside the cushion which provides a lifting force on the vessel which decreases the draft. This lifting force may account for up to 80 % of the weight of the vessel, whereas the remaining buoyancy is provided by the displaced side-hulls. Such a decrease in vessel draft results in only a small portion of the vessel being

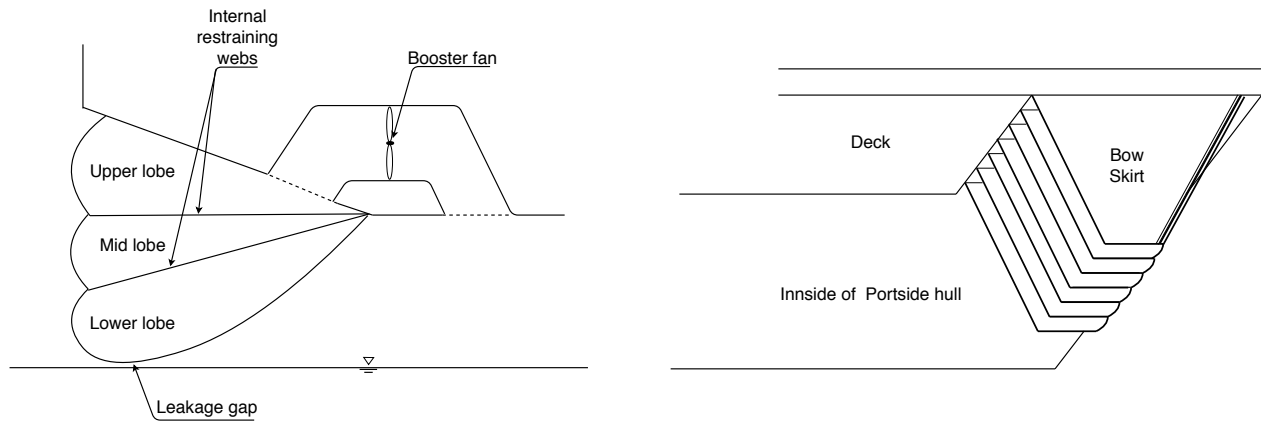


Figure 1.3: Left: Stern bag configuration, Right: Individual fingers making up the bow skirt

submerged, which provides a great reduction in water resistance, making it capable of reaching greater velocities than a similar sized catamaran structure with moderate propulsive power consumption.

The fact that the pressurized cushion holds a greater pressure than the environment, causes a lowering of the water level inside the cushion (Figure 1.4). This effect has implications for the rolling motion of the vessel, as a change in water plane area inside the cushion has a destabilizing effect for the roll-restoring moment (Faltinsen (2005)).

Compared to Air Cushion Vehicles (ACVs), for example a hovercraft, the directional stability is greater due to the displacement of the catamaran side-hulls. The fact that these hulls are submerged, facilitate the use of high-speed vessel propulsion systems like a water-jet.

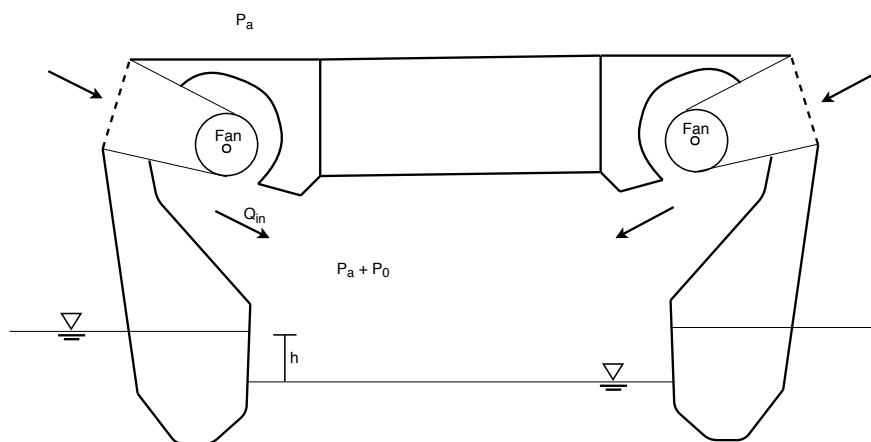


Figure 1.4: SES cross section displaying water level inside and outside of the hull

For the purpose of this thesis, the vessel concerned is based on the WAVECRAFT™ developed by UMOE Mandal. This vessel carries about twice the lift fan capacity of a like-sized conven-

tional SES. In addition to the increased lift capacity, *vent valve louvers* are fitted which enable the cushion leakage area, A_l , to be controlled. Leakage through the vent valve louvers (*louver leakage*) differs from the aforementioned leakage around the bow and stern seals, denoted *passive leakage*, in the sense that the louver leakage introduces a way of actuating the cushion pressure in addition to the lift fan speed. Changing the leakage area using the vent valves introduce an active way of altering the cushion pressure more rapidly than by alterations to the fan speed, which enables the cushion pressure to be actuated at relevant sea wave periods (3-12 seconds).

1.1.3 Related Work

Ever since the first vessels were launched in the 1960s, several comprehensive studies regarding the SES have been done. Due to the unique characteristics of the vessel; i.e the air cushion, catamaran hull, lift fan and ventilation system which result in some novel effects compared to conventional vessels, research on the SES is of interest both in a control theory and hydrodynamic perspective. The motivation behind the research lies in the possibilities of creating a versatile vessel of low environmental impact, with capabilities such as motion control in the vertical plane and high speeds.

This section will present an overview of some of the research done on the SES, with a focus on building a mathematical description and applications of different means of control.

An early study on the special characteristics of the SES with regards to hydrodynamic aspects is found in Kaplan and Davis (1974) and Kaplan et al. (1981). As the development of the SES still was in its early stages, investigations on the dynamic response characteristics and novel phenomena inflicted by the air-cushion and hull-shape were performed. New techniques were developed with implications for SES design, and a simplified mathematical model of the SES dynamics was established which served as the foundation for further development in the years to follow.

This comprehensive study addresses issues such as fluctuations in cushion pressure, air leakage, body-fluid interactions and power requirements, and is able to link this dynamic behavior contained in a mathematical description (Equation: 1.1), which showed good correlation with full-scale tests. Basic equations of motion for heave and pitch are respectively given by:

$$\begin{aligned}
m\ddot{z} + A_b P_0 \mu - Z_{\dot{z}} \dot{z}_3 - Z_z z - Z_{\dot{\theta}} \dot{\theta} - Z_{\theta} \theta &= Z_{waves}(t) \\
I_{yy} \ddot{\theta} - A_b p_0 x_{CP} \mu - M_{\dot{\theta}} \dot{\theta} - M_{\theta} \theta - M_{\dot{z}} \dot{z} - M_z z &= M_{waves}(t),
\end{aligned} \tag{1.1}$$

where m is the vessel mass, I_{yy} is the moment of inertia about the pitching axis, z and θ is motion in the heave and pitch degree of freedom, Z and M derivatives represent different hydrostatic and hydrodynamic coefficients, Z_{waves} and M_{waves} is the hydrodynamic excitation force and moment in heave and pitch, A_b is the air cushion area, p is the gauge cushion pressure, p_0 is the cushion equilibrium pressure, $\mu = \frac{p-p_0}{p_0}$ is the dynamic uniform cushion pressure variation and x_{CP} is the distance between the cushion center of pressure and vessel center of gravity.

Kaplan and Davis (1974) also present the following equation for the linearized cushion pressure by combining the flow in and out of the cushion, in addition to an adiabatic pressure-density relation:

$$K_1 \dot{\mu} - \rho_a A_b \dot{z} + \rho_a A_b x_{CP} \dot{\theta} = -K_3 \mu - K_2 \Delta A_l - \rho_a \dot{V}_{b,waves}(t), \tag{1.2}$$

where $K_1 = \frac{\rho_a A_b h_b}{\gamma(1+\frac{p_a}{p_0})}$, $K_2 = \rho_a c_n \sqrt{\frac{2p_0}{p_a}}$, $K_3 = \frac{\rho_a Q_0}{2} - \rho_a \left(\frac{\partial Q}{\partial p}\right)_0 p_0$, ρ_a is the density of air, ΔA_l is the controlled leakage area, $\dot{V}_{b,waves}$ is the wave volume pumping, h_b is the cushion height, C_n is the orifice coefficient, p_a is the atmospheric pressure, γ is the specific heat ratio for air, Q_0 is the fan flow rate at equilibrium pressure P_0 , and $\left(\frac{\partial Q}{\partial p}\right)_0$ is a linearization of the fan slope. The relations presented in equations 1.1 and 1.2 provide the basis for the state space model presented in section 2.6.2.

Another topic of interest presented by Kaplan et al. (1981) with regards to this thesis, is their analysis on designing a Ride Control System (RCS). By using different means of altering the pressure of the air cushion, it was found that a ride control system could reduce vertical plane accelerations of the vessel. Multiple approaches for actuation were investigated; either by changing the flow into the cushion by changes to the fan input area, fan speed or controlling the fan blade angles, or adjusting the outflow using ventilation louvers. The control law used is similar to the one used in this thesis; usage of a control signal proportional to the vertical velocity. The requirements of additional lift-fan capacity for actuation of the cushion is also discussed along with signal processing and nonlinearities in the actuators.

The potential of the RCS is further investigated in Adams et al. (1983) with application oriented towards a 200-ton U. S. Navy SES. For this usage, a decrease in range as a consequence of increased average draft due to the varying cushion pressure is found. However, the advantages of reduced vertical accelerations are considered greater with regards to the benefit of reduced crew fatigue and efficiency. Using both digital and analog implementations of a similar control

law as in Kaplan et al. (1981) with vent valve louvers as actuators, they conduct a series of tests both on a simulation model and the full-scale vessel. They obtain results of the control system at different vessel speeds which are used for predictions towards the scalability of the system to vessels of different sizes.

Of particular relevance is their discussion of controller gains, which is set manually in these experiments. They find that the effectiveness of the system starts to level out at a certain threshold, where excessive saturation leads to the vent valves either being fully open or fully closed at a large extent of time. The point of where this threshold is found, varies between sea-states, due to the sea-state-dependant nature of the feedback control law. It was also found that increasing the lift capacity in combination with an increased number of vent valves, further increased the performance of the system. The cost of added hydraulic power required to actuate the vent valves are modest due to relatively light loads on the vent-valves from the exhausting flow of air. However, the added cost of powering the lift fans while releasing the pressure to support the RCS was found to be quite significant. Particularly for higher sea conditions where tests showed that the flow of air through the vent valves on average accounted for two-thirds of the flow from the fans.

Equation 1.2 is based on the assumption that the cushion pressure is spatially uniform throughout the cushion. Moran (1975) and Moran (1976) examine the validity of this assumption through experiments where pressure measurements are conducted in the cushion of a high length-to-beam ratio SES subjected to both regular and irregular waves of different amplitudes and frequencies.

Experiments were performed by comparing recordings of the incident wave to the response of the vessel, where a lack of regularity was found both in the change in magnitude of the pressure as well as the development of the phase lag. The previously used assumption had been that waves pass underneath the vessel, emerging exactly as they entered. However, the experiments conducted by Moran falsify this assumption, experimentally showing that the cushion pressure is not uniformly distributed, which leads to unidentified dynamics in the concurrently used mathematical models.

The effects of the spatially varying cushion pressure are further investigated in Steen (1993) and Sørensen et al. (1993). The former presents a study of the impact of the *Cobblestone effect* on a SES using full-scale measurements and establishing a mathematical model for the first acoustic modes of the resonant oscillations, while the latter extends this mathematical model to consider an infinite number of acoustic modes and focus on the implications for the RCS.

The Cobblestone effect is high-frequency vertical accelerations due to the excitement of acous-

tic modes of the air cushion. This effect is dominating at low wave amplitudes and high velocities, as the *encounter frequency* is high and the surpassing waves cause rapid variations in the cushion volume. A result of this phenomenon is vertical vibrations which may cause a large degree of discomfort among the crew and passengers.

Experiments discovered three distinct frequencies below 10Hz where these accelerations would appear (Steen (1993)). The lowest frequency would correspond to the resonant frequency of the dynamic cushion pressure which was well-known and accounted for in existing models. However, the source of resonance for the other frequencies, which were previously unknown, were discovered to come from the spatially varying cushion pressure. The work of Sørensen and Steen provided a new mathematical description of the vertical plane SES dynamics, which incorporated the effects of spatially varying cushion pressure by use of modal analysis. It was found that for higher frequencies (above 5Hz) the spatial cushion variations are dominant, whereas towards lower frequencies, the uniform cushion pressure becomes increasingly dominant. To be able to control and dampen the spatially varying resonances, a high servo-frequency response is required for the hydraulic-electric vent valve servo system.

This work also comprises of comparing configurations of flexible aft seals to rigid seals, where it was found that the configuration with the flexible seals experiences larger vertical accelerations which is explained by the difference in leakage gap. This, in turn, affects the magnitude and frequencies of where the spatially varying cushion pressure cause vibrations, and it is found that the rigid seals cause the resonant response to be lower and appear at higher frequencies. Placement of the inlet fans and ventilation valves relative to the cushion in the longitudinal direction was also shown to be of impact on the oscillations, where it is found that placing the in- and outlets towards one of the far ends of the cushion increases damping.

The effect of a flexible stern bag on the Cobblestone oscillations is further investigated in Ulstein (1995). Deformations of the bag due to the air pressure in the bag, the cushion pressure and hydrodynamic loads on the wetted surface of the flexible bag, cause non-linear variations in the leakage area and cushion volume for a vessel exposed to waves. Results show that a 2-loop stern seal bag is able to reduce the first spatial resonance frequency from 6 to 5Hz compared to a rigid seal, due to how the flexible seal is able to more closely follow the water surface to minimize the air leakage.

The extended mathematical model incorporating the effects of acoustic resonances is used to derive a new control system whose objective is to provide dampening of both the dynamic uniform pressure and effects from the spatially varying pressure. In Sørensen and Egeland (1995) such a new ride control system is designed with use of *dissipative control*. The idea is that by dissipating energy at the resonant frequencies of the spatial pressure variations, the resulting verti-

cal accelerations are dampened. Simulations using the model including the contributions from the first three acoustic modes, in addition to full-scale tests showed significant improvements in ride quality at moderate to high speeds. Note that the effects of spatially varying pressure oscillations are a concern at high speed with high encountered frequencies. This is not included in the control system described by this thesis, which deals with a vessel operating at zero speed.

A crucial component of any heave-compensated system (such as the BCS) is obtaining sufficient quality measurement signals for the controller. K uchler et al. (2011) contains a vessel-general description on using an observer based on signals from an inertial measurement unit (IMU) to estimate the vertical motions. The observer functions by applying a Fourier transform to the acceleration signals supplied by the IMU to establish an energy density spectrum. The spectrum presents the wave energy content over a frequency range, which is used to identify the size and frequency of the different wave components. The wave motion is then predicted by a sum of sine waves (modes) corresponding to the most significant frequencies in the spectrum. The accuracy of the estimation is dependant on the number of modes included in the prediction. The observer is realized as an extended Kalman filter to limit noise, and is chosen to penalize modes of a higher eigenfrequency rather than lower ones. The heave motion is estimated by using the response amplitude operator (RAO) which is a transfer function depicting the vessel response at different frequencies.

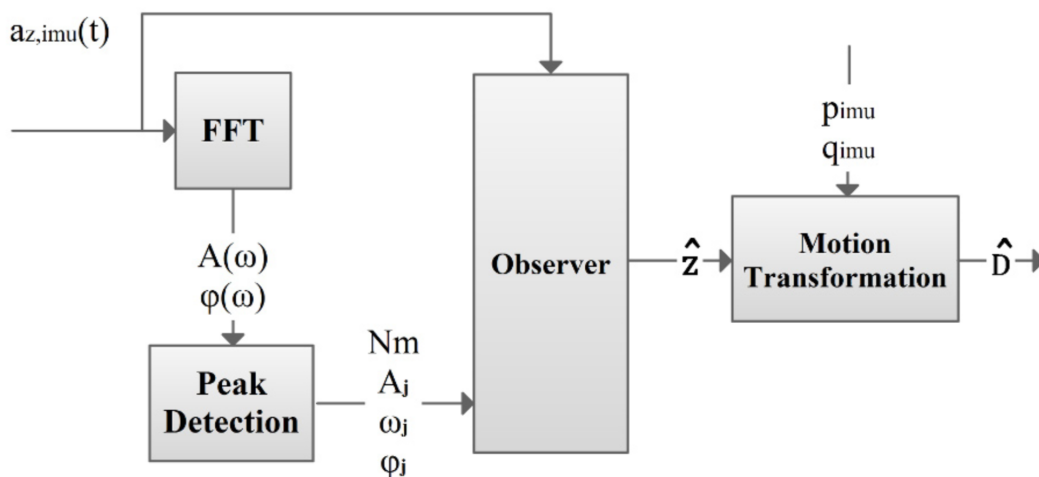


Figure 1.5: Heave Estimation Scheme (Auestad et al. (2013a))

Auestad et al. (2013a) presents an approach of heave motion estimation closely based on the workings of K uchler et al. (2011). An overview of the estimation scheme is presented in Figure 1.5. This approach is more directly concerned with the application for providing input signals for the BCS on a WAVECRAFTTM surface effect ship. In particular, proper estimation of the mo-

tions at the vessel bow is of concern. The paper considers two main approaches of obtaining this signal: A direct approach with the IMU located near the bow, and an indirect approach placing the IMU at the midship and calculating the bow movements through motion transformation.

This paper emphasizes some of the challenges faced when attempting motion estimation of a surface effect ship. In particular, the vibrations caused by the lift fan pose process disturbances on the signals, which set great requirements for the filtering capabilities of the observer. These disturbances are found to be even greater when placing the IMU near the bow, such that the approach of calculating the bow-motions using measurements made midships and applying a motion transformation is recommended and the observer scheme is concluded to provide usable inputs for a controller.

Auestad et al. (2013b) introduces a simulation model for a SES. The model is based on the previously existing mathematical description Faltinsen (2005) with the incorporation of the effects of flexible rubber bow and stern seals. The paper does not discuss the previously mentioned acoustic resonance oscillations, as the focus is describing the dynamics at zero speed and the vessel is small enough such that these effects are not experienced. The paper also introduces a simplified control plant model (CPM) whose purpose is describing only the dynamics of the plant characteristics relevant to the control problem; heave, pitch and uniform pressure variations. The introduced feedback controller is designed to minimize the vertical motion of the bow of the vessel, as means of facilitating the boarding procedure at offshore wind turbines.

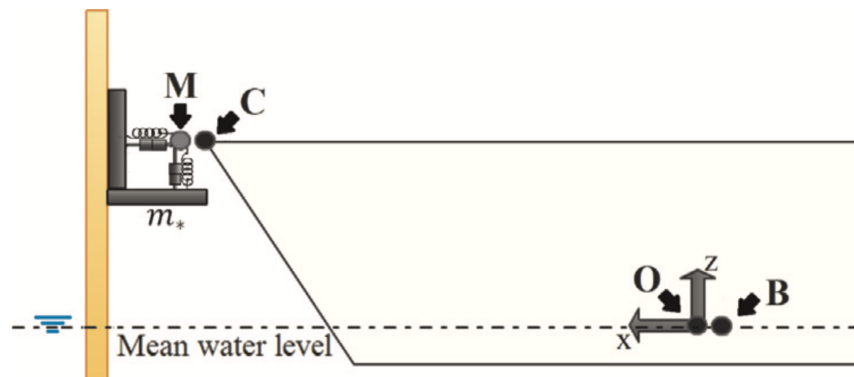


Figure 1.6: Modeling of turbine contact (Auestad et al. (2015))

In addition to the damping injected by the control of vent valves, Auestad et al. (2015) presents an additional feature to further decrease the vertical accelerations of the bow; utilizing and modeling the friction force between the turbine and the bow itself. By applying propulsion force to achieve physical contact between the bow and the turbine, and actuation through the vent valves, the *Boarding Control System* (BCS) introduces a way of achieving increased accessibility not only to wind turbines, but to other offshore structures with a similar docking procedure.

Forces between the bow and turbine are implemented in the simplified model as a vertical and horizontal spring force (Figure 1.6) which differentiates between when the relative motion between the bow and turbine is above a certain threshold (kinetic friction), and when the bow and turbine stick together (static friction). Both simulation results and full-scale testing at sea states up to $H_s 2.5 m$ have proven the efficiency of the boarding control system at achieving increased accessibility.

Application of adaptive control to the SES has previously been investigated by Basturk (2013) where an acceleration feedback approach was made to reduce ramp motions between a SES and a large RORO-vessel positioned side by side to provide a safer environment for cargo transfer between the ships. The focus lied with minimizing the motions at the connection point of the ramp at the SES midship, by using the louver area as an actuator. An adaptive backstepping controller which estimates the unknown disturbances on a LTI system of both known and unknown parameters from measurements of pressure, heave rate and accelerations is developed. Basturk (2013) also include a comprehensive stability analysis of the closed-loop system, in addition to verification through model tests. The non-linear cushion model described later in this thesis makes developing such an adaptive controller difficult. However, by introducing some simplifications such as decoupling of heave and pitch in the model they are able to realize a controller whose results show great motion damping capabilities. This work focuses on providing a mathematical description of the adaptive control system with emphasis on proving controller stability and simulations, as opposed to this thesis whose purpose is using an adaptive approach to find controller parameters for an existing feedback controller. The vessel model implemented also use a split-cushion configuration which renders the capability of actuating the heave and pitch degree of freedom simultaneously.

Chapter 2

Mathematical Modeling

This section will contain a mathematical description of the dynamics which lay the ground for the simulation models. Similar to other marine vessel models is the knowledge requirement of the rigid body kinematics, as well as a way of rendering disturbances which in this case is the environmental loads. Specific for the SES vessel type is the introduction of the air cushion dynamics and its implications on the vessel response.

The degree of which details of the dynamics are included in the model determines the ability of the model to act as a representation of the real-life vessel. For this thesis, two models are used; a *process plant model* called SESSim developed by UMOE Mandal which is designed to capture most of the subtle details of the SES dynamics for a wide range of operating conditions. Additionally, a *control plant model* based on Auestad et al. (2015) is used. This model contains some simplifying assumptions and neglects some effects which weaken the ability to capture the real-life system, but has implemented the dynamics required for the purpose of control development.

2.1 Coordinate Frame

The process plant model is a 6 degree of freedom model. However, the focus of this thesis is the vertical motion of the vessel when exposed to waves and the contribution from the cushion pressure. The forces from the cushion pressure are derived in a *body-fixed* reference frame, as they follow the rotation of the vessel. Wave induced vessel motions are derived in a seakeeping reference frame which follows the vessel forwards and to the sides but remain parallel to the mean water surface. Figure 2.1 depicts the notation that will be used when describing the vessel,

with the rotation around the y-axis, the pitching motion, η_5 and the translation along the z-axis, η_3 being given attention in this thesis.

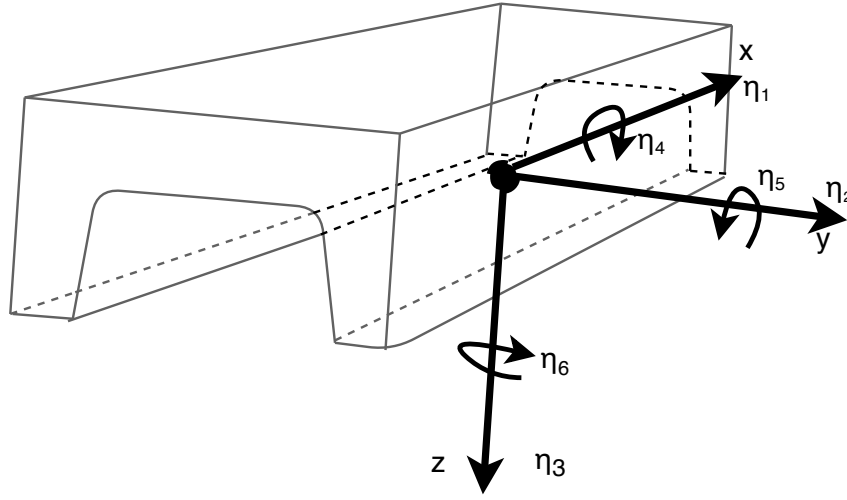


Figure 2.1: *Coordinate system definition*

2.2 Equation of Motion

Following Faltinsen (1990), the motion of any point of the body can be written as

$$\mathbf{s} = \eta_1 \mathbf{i} + \eta_2 \mathbf{j} + \eta_3 \mathbf{k} + \boldsymbol{\omega} \times \mathbf{r}, \quad (2.1)$$

where \mathbf{i} , \mathbf{j} and \mathbf{k} are the unit vectors along the x , y and z axis, $\boldsymbol{\omega} = \eta_4 \mathbf{i} + \eta_5 \mathbf{j} + \eta_6 \mathbf{k}$ and $\mathbf{r} = x \mathbf{i} + y \mathbf{j} + z \mathbf{k}$. This yields:

$$\mathbf{s} = (\eta_1 + z\eta_5 - y\eta_6) \mathbf{i} + (\eta_2 - z\eta_4 + x\eta_6) \mathbf{j} + (\eta_3 + y\eta_4 - x\eta_5) \mathbf{k}. \quad (2.2)$$

As the concern of this thesis is vertical motions, and disregarding the roll degree of motion as it is not controlled in this thesis, the following expression for the total vertical motion is found as:

$$s_3 = (\eta_3 - x\eta_5). \quad (2.3)$$

A general expression for the 6 DOF motion can be found as:

$$\sum_{k=1}^6 [(M_{jk} + A_{jk}) \ddot{\eta}_k + B_{jk} \dot{\eta}_k + C_{jk} \eta_k] = F_j, \quad j = 1, 2, \dots, 6, \quad (2.4)$$

where M_{jk} is inertia, A_{jk} is the added mass coefficient, B_{jk} is the damping coefficient, C_{jk} is the restoring coefficient and F_j is the forces acting in their representative degrees of freedom both from the air cushion and environmental loads.

2.3 Pressure Dynamics

A model for the cushion pressure dynamics is a vital component in the description of the SES. A mathematical description of the cushion dynamics is first found in Kaplan et al. (1981) which captures the key aspects of the implications of the air cushion, but with some simplifying assumptions such as the cushion pressure being uniformly distributed and ignoring some coupling effects. Sørensen and Egeland (1995) contains a mathematical description which includes the effects of spatial pressure variations which is crucial when accounting for the Cobblestone oscillations occurring at high speeds. For the purpose of this thesis however, the concern is modeling the cushion dynamics at zero forward speed such that the uniform pressure assumption is valid.

The following derivation of the cushion dynamics is based on Faltinsen (2005) but including coupling and non-linear effects which is coherent with the implementation in the numerical simulation model (SESSim) provided by UMOE Mandal which has been verified using full-scale tests. A simplification of the cushion dynamics is later implemented in a *control-plant model*, which implies losing some of the ability to capture the dynamics of the full-scale vessel, but sufficient for the purpose of testing and designing a control system.

Figure 2.2 depicts the *control-volume* (CV) making up the air cushion. By starting with the continuity equation for the air inside the cushion the following relation is obtained (Sørensen et al. (1993)):

$$\rho_a(Q_{in}(t) - Q_{out}(t)) = \frac{1}{L} \frac{\partial}{\partial t} \left(\int_{-L/2}^{L/2} \rho_c(x, t) V_c(t) dx \right). \quad (2.5)$$

Here, $Q_{in}(t)$ is the volumetric flow of air into the cushion, $Q_{out}(t)$ is the volumetric flow out of the cushion, ρ_a is the air density at equilibrium pressure, $\rho_c(x, t)$ is the density of air inside the cushion distributed longitudinally, and $V_c(t)$ is the air cushion volume.

Disregarding the spatial dependency of the density of air in the cushion, ρ_c , by assuming a uniform pressure distribution yields

$$\rho_a(Q_{in}(t) - Q_{out}(t)) = \dot{\rho}_c(t) V_c(t) + \rho_c(t) \dot{V}_c(t). \quad (2.6)$$

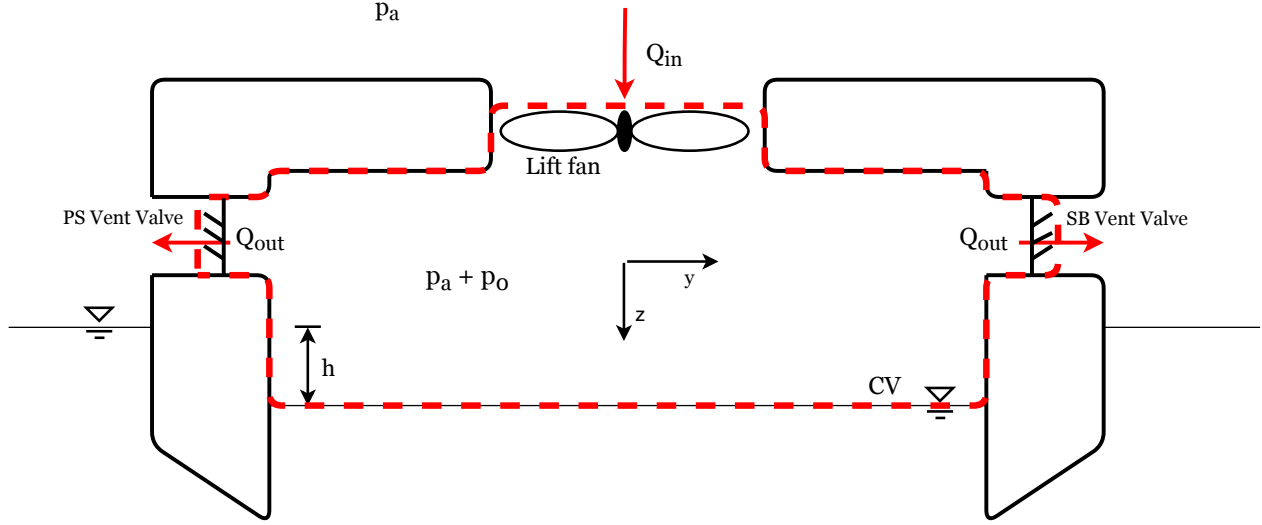


Figure 2.2: Control volume boundaries for the air cushion

The lift fan pump characteristics determine the flow of air into the cushion, Q_{in} . The *pump-curve* (Figure 2.3) depicts how the fan flow rate may vary with the cushion pressure for one set RPM of the fan. This thesis does not utilize varying fan speed as means of actuation, so the fan speed is kept constant which means only one constant pump curve is of concern. Figure 2.3 also depicts how the pump curve is linearized around some operating point $(Q_{in,0}, p_0)$ which yields the linear slope $\frac{\partial Q}{\partial p}|_0$. This simplification is later used in the control plant model and sufficient at small pressure variations. For the SESSim-model however, the true curve is implemented for a range of fan operating speeds. A configuration with multiple pumps is also possible by adding together the contribution from each pump

The term Q_{out} captures both the active leakage through the vent valves and passive leakage through the seals. The total flow out of the cushion is given by

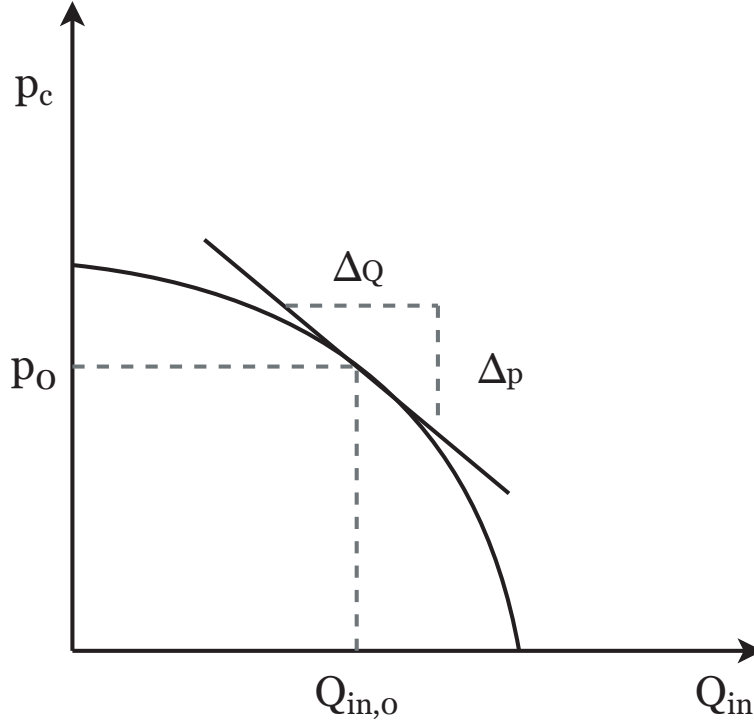
$$Q_{out} = c_n A_L \sqrt{\frac{2p_u}{\rho_a}}, \quad (2.7)$$

where the total leakage area A_L is defined as

$$A_L = A_{L,passive} + A_{L,active}. \quad (2.8)$$

C_n is the orifice coefficient for capturing air flow losses due to the vent valve duct shape, seals and hull.

The relation between pressure and density is assumed adiabatic, which means the cushion air

Figure 2.3: *Lift fan pump-curve*

density can be expressed as

$$\rho_c(t) = \rho_a \left(\frac{p_a + p_u(t)}{p_a + p_0} \right)^{\frac{1}{\gamma}}. \quad (2.9)$$

Here, $p_u(t)$ is the uniform dynamic cushion pressure, p_0 is the equilibrium pressure and γ is the specific heat ratio for air.

The cushion volume V_c is a function of the vertical position z , cushion area A_c , pitch angle θ and wave volume pumping V_0 and can be expressed as

$$V_c(t) = A_c(t)(h_0 - z(t) + x_{cp}(t)\theta(t)) - V_0(t), \quad (2.10)$$

which differentiates into

$$\dot{V}_c = A_c(t)(x_{xp}(t)\dot{\theta} + \dot{x}_{cp}\theta(t) - \dot{z}) - \dot{V}_0. \quad (2.11)$$

Here, x_{cp} is the distance between the longitudinal center of gravity to the cushion center of pressure.

Sørensen (2013) presents the following expression for wave volume pumping which is used in the control plant model:

$$\dot{V}_0(t) = b \int_{-L/2}^{L/2} \dot{\zeta}(x, t) dx, \quad (2.12)$$

where b is the cushion width and ζ is the wave amplitude inside the cushion. This expression does not account for the wave volume pumping due to vessel excitations in heave and pitch. To capture these effects the process plant use the following expression for the total volume pumping:

$$\dot{V}_c = A_c(t)x_{cp}(t)\dot{\theta} - A_c(t)\dot{z} + b \int_{-L/2}^{L/2} \dot{\zeta}(x, t) dx. \quad (2.13)$$

By combining the terms in 2.6 and 2.9 and differentiating with respect to time then the following differential relation for the dynamic cushion pressure emerges:

$$\dot{p}_u = \frac{\gamma(p_a + p_u(t))}{V_c(t)} \left(\left(\frac{p_a + p_0}{p_a + p_u(t)} \right)^{\frac{1}{\gamma}} (Q_{in}(t) - Q_{out}(t)) - \dot{V}_c \right). \quad (2.14)$$

2.4 Environment

The simulations of the SESSim model are performed in the Marine Systems Simulator (MSS), which is a framework for testing mathematical models of marine systems (Perez et al. (2006)).

The MSS has capabilities of replicating a range of different sea states with user input of the governing parameters. For this thesis, simulations are done for regular waves and irregular waves generated from the *Jonswap*-spectrum. As irregular waves have implications for the heave control system, irregular waves generated from the Jonswap spectrum was implemented to the simplified control plant model as well.

The Jonswap spectrum is generated by the following formulation (Det Norske Veritas (2011)):

$$S(\omega) = A_\gamma S_{PM}(\omega) \gamma \exp\left(-0.5 \left(\frac{\omega - \omega_p}{\sigma \omega_p}\right)^2\right), \quad (2.15)$$

where S_{PM} is the *Pierson-Moskowitz* spectrum defined by

$$S_{PM}(\omega) = \frac{A}{\omega^5} \exp\left(-\frac{B}{\omega^4}\right) \quad A = 0.0081 g^2, \quad B = 0.74 \left(\frac{g}{V}\right)^4. \quad (2.16)$$

Here, V is the wind-speed at 19.5m altitude, γ is a non-dimensional peak shape parameter usually set to 3.3, $A_\gamma = 1 - 0.287 \ln(\gamma)$ is a normalizing factor and σ is a spectral-width parameter defined by $\sigma = \sigma_a = 0.07$ for $\omega \leq \omega_p$ and $\sigma = \sigma_b = 0.09$ for $\omega > \omega_p$. ω_p is the *peak-frequency* of the spectrum which states what frequency holds the most energy.

The wave elevation is generated by superposition of the contribution from the different frequen-

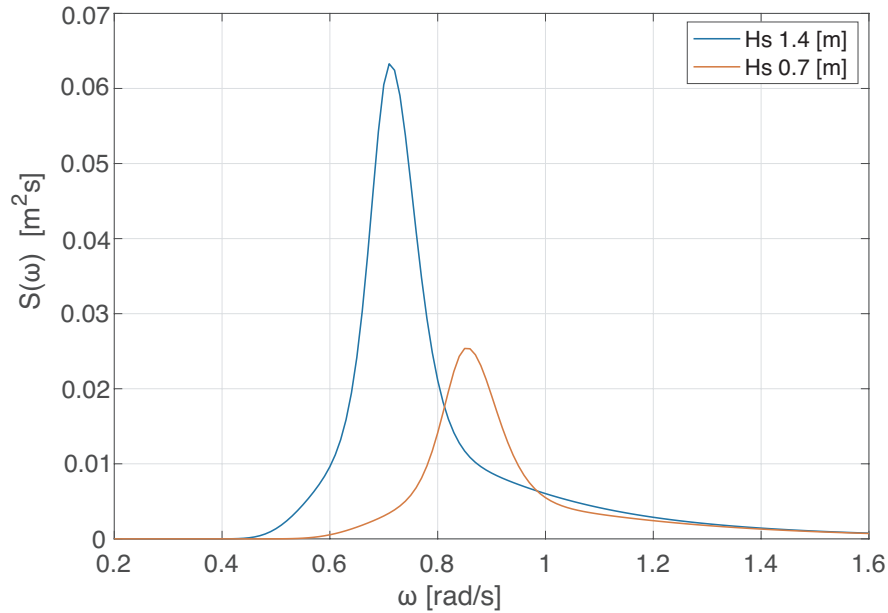


Figure 2.4: Realization of Jonswap spectra

cies and adding a random phase angle ϵ according to:

$$\zeta_a = \sum_{i=1}^n A_i \sin(\omega_i t + \epsilon) \quad A_i = \sqrt{2S(\omega_i)d\omega_i}, \quad (2.17)$$

where n is the specified number of wave frequencies and $d\omega$ is the range between each frequency.

Wave series containing a transition between sea states is generated by defining a point in time for the transition to start, the duration of the transition and updating the wave spectrum during the transition. Figure 2.4 depicts the initial and final state of the spectrum before and after a transition.

After running simulations, it became apparent that when defining the frequencies of where the waves are generated from, if a limited number n of equally spaced frequencies was selected, a repeating structure in the wave series would appear. This is due to how a specific frequency would coincide with other frequencies regularly. To counteract this effect, a small random perturbation could be added to each frequency such that the smallest common denominator between the selected frequencies would be larger. The effect of this is apparent in figure 2.5 with sea states drawn from the same spectrum but with a slightly different selection of frequencies.

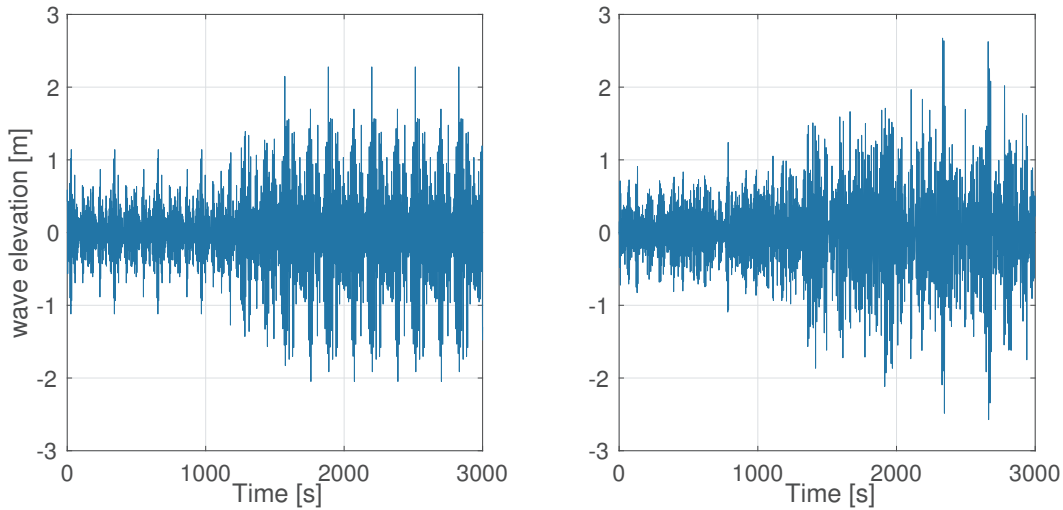


Figure 2.5: *Left: Wave-series with equally spaced frequencies and repeating structure, Right: Wave-series with noise added to the selection of frequencies*

2.5 SESSIM - Process Plant Model

The SESSim-model is an expansion of the MSS simulation environment (Perez et al. (2006)) where the rigid body dynamics of the vessel have been calculated using the ship design tool *ShipX* and the vessel response plugin *VeRes* (Fathi and Hoff (2004)). Hydrostatic and dynamic coefficients are calculated using strip theory and response amplitude operators (RAOs) are calculated for a set of linearized wave loads with the input of vessel dimensions, mass distribution, radii of gyration and velocity. The RAO is a transfer function able to relate the exciting forces at different frequencies to the resulting vessel response. The disturbance model in the MSS generates a wave signal with a predefined number of frequencies. The RAO is then used to calculate the corresponding wave forces at each frequency which are then superimposed to obtain the incident wave force. Added to the model are the forces from the air cushion, which is based on the non-linear pressure equation (equation: 2.14).

By knowing the forces acting upon the vessel and its response characteristics, the vessel motion is obtained. Fossen and Smogeli (2004) present a time-domain model developed from the *Cummins equation* (Cummins (1962)) which the SESSim model is based on. It includes fluid memory effects which makes it valid for different sea states and capable of taking wave excitation forces as inputs. It is also on a state-space form which makes it suitable for control system design (Perez et al. (2004)). The SESSim model also includes linear and non-linear damping effects where the coefficients are found using *VeRes* calculations and empirical model tests on the *WAVECRAFT™*. The model is stated as:

$$\begin{aligned}
(\mathbf{M} + \mathbf{A}_\infty)\dot{\mathbf{v}} + \mathbf{D}_{linear}\mathbf{v} + \mathbf{D}_{nonlinear}\mathbf{v}|\mathbf{v}| + \boldsymbol{\mu} + \mathbf{G}\boldsymbol{\eta} &= \boldsymbol{\tau}_{env} + \boldsymbol{\tau}_{cushion} \\
\dot{\boldsymbol{\eta}} &= \mathbf{J}_\Theta(\boldsymbol{\eta})\mathbf{v}
\end{aligned} \tag{2.18}$$

where:

- $\mathbf{M} \in \mathbb{R}^{6 \times 6}$ is the rigid body mass matrix.
- $\mathbf{A}_\infty \in \mathbb{R}^{6 \times 6}$ is a constant generalized added mass matrix evaluated at the infinity frequency.
- $\dot{\mathbf{v}} \in \mathbb{R}^{6 \times 1}$ is the linear and angular velocities in the body-fixed reference frame.
- $\mathbf{D}_{linear} \in \mathbb{R}^{6 \times 6}$ is the linear viscous damping matrix from VeRes calculations.
- $\mathbf{D}_{nonlinear} \in \mathbb{R}^{6 \times 6}$ is the non-linear viscous damping matrix where the coefficients are tuned from curve-fitting the results of model decay tests.
- $\mathbf{G} \in \mathbb{R}^{6 \times 6}$ is a matrix of linear generalized gravitation and buoyancy force coefficients.
- $\boldsymbol{\eta} \in \mathbb{R}^{6 \times 1}$ is a vector of positions and orientations in an *earth-fixed* reference frame.
- $\boldsymbol{\tau}_{env} \in \mathbb{R}^{6 \times 1}$ is a vector of environmental loads and moments from the RAO.
- $\boldsymbol{\tau}_{cushion} \in \mathbb{R}^{6 \times 1}$ is a vector of forces and moments from the air cushion pressure.
- $\mathbf{J}_\Theta(\boldsymbol{\eta})$ is a kinematic transformation matrix for linear and rotational velocities from the body-fixed frame to the earth-fixed frame.

$\boldsymbol{\mu} \in \mathbb{R}^{6 \times 1}$ is a potential damping term described by the following state-space model (Kristiansen and Egeland (2013)):

$$\begin{aligned}
\dot{\boldsymbol{\chi}} &= \hat{\mathbf{A}}\boldsymbol{\chi} + \hat{\mathbf{B}}\mathbf{v}, \boldsymbol{\chi}(0) = 0 \\
\hat{\boldsymbol{\mu}} &= \hat{\mathbf{C}}\boldsymbol{\chi} + \hat{\mathbf{D}}\mathbf{v}
\end{aligned} \tag{2.19}$$

where $\hat{\mathbf{A}}$, $\hat{\mathbf{B}}$, $\hat{\mathbf{C}}$, and $\hat{\mathbf{D}}$ are constant matrices of appropriate dimensions.

The SES-specific dynamics are implemented with the intention of matching the real-world vessel as closely as possible. Acceleration measurements are available, but they are treated with noise of similar magnitudes and frequencies as accelerometers on the full-scale vessel experience. Actuation of the system is obtained by altering the commanded vent valve leakage area. This signal is input to a transfer function whose purpose is mimicking the response of the servo which controls the hydraulics actuating the vent valves.

Passive leakages are accounted for by adding up the estimated leakage areas from three components based on knowledge of the hull and seal geometry: hull leakage by evaluating the heave position compared to the draft at equilibrium, bow and stern leakage due to heave by evaluating the heave position compared to knowledge of draft and seal dimensions, and leakage under the bow seal due to pitch from evaluating the pitch angle and location of the lower bow finger tips.

Multiple tests performed on model- and full-scale vessels are used to verify the ability of the SESSim of capturing the dynamics of the WAVECRAFT™. Cushion pressure response for varying vent valve openings, inclination tests and coupled heave and pitch response in waves all show that the SESSim is capable of a highly accurate resemblance of the real world vessel.

2.6 Simplified Control Plant Model

The purpose of the control plant model is to provide a simulation environment for the development of a control system. The model needs to be sufficiently accurate in capturing the relevant dynamics subject to control, but is not required an equally degree of accuracy towards the real-life system as the SESSim model.

This model is based on Auestad et al. (2015) which was used in the development of the BCS.

2.6.1 Linear Pressure Model

Control of the system is based on adjusting the leakage area of the air cushion $A_L(t)$ which is assumed proportional to the air outflow Q_{out} for the control plant model. Air inflow Q_{in} is supplied by fans running at a constant speed. The model is linearized around a certain air cushion equilibrium pressure P_0 , for a given vessel draft d . The hydrodynamic and hydrostatic coefficients of the vessel are assumed constant and are based on this draft condition. The following model statement for the air cushion pressure model follows Sørensen and Egeland (1995).

To allow controller outputs to be both positive and negative, the leakage area is centered about some mean operating value A_0 , while the actual control parameter $A_L(t)$ represents any deviation in leakage area from A_0 . The true leakage area is given by:

$$A_L(t) = A_0 + \Delta A_L(t). \quad (2.20)$$

With a constant leakage area of A_0 and no waves, the cushion pressure will reach the equilib-

rium pressure P_0 , which is the sum of P_a , the atmospheric pressure and P_u , the excess air cushion pressure at equilibrium. To capture the excess cushion pressure variations over time $P_u(t)$, related to the equilibrium pressure, $\mu_u(t)$ is defined as a uniform non-dimensional dynamic cushion pressure variable where

$$\mu_u(t) = \frac{P_u(t) - P_0}{P_0}. \quad (2.21)$$

Using this definition, the dynamics for the linear pressure variable can be expressed using the following differential relation:

$$K_1 \dot{\mu}_u(t) + K_3 \mu_u(t) + \rho_{c0} A_c \dot{\eta}_3(t) - \rho_{c0} A_c x_{cp} \dot{\eta}_5(t) = K_2 \Delta A_L(t) + \rho_{c0} \dot{V}_0(t) \quad (2.22)$$

$$K_1 = \frac{\rho_{c0} h_0 A_c}{\gamma \left(1 + \frac{P_a}{P_0}\right)}, \quad K_2 = \rho_{c0} C_n \sqrt{\frac{2P_0}{\rho_a}}, \quad K_3 = \frac{\rho_{c0}}{2} \left(Q_0 - 2P_0 \left. \frac{\partial Q_{in}}{\partial P} \right|_0 \right).$$

Here, ρ_{c0} and ρ_a is the equilibrium cushion density and the ambient air density respectively, h_0 is the cushion height, A_c is the cushion area, γ is the heat capacity ratio of air, C_n is the orifice coefficient for the vent valve duct shape, Q_0 is the equilibrium cushion air flow rate, $\left. \frac{\partial Q_{in}}{\partial P} \right|_0$ is the linearized lift fan characteristic slope at the equilibrium point and x_{cp} is the distance between the origin of the inertial reference frame and the center of the air cushion in the longitudinal direction. $\dot{V}_0(t)$ represents the changes in cushion volume due to sea wave pumping, which causes a disturbance in the dynamic pressure (see equation 2.12).

2.6.2 State Space Model

The equations of motion follow Equation 2.4 and are stated in heave and pitch as

$$(m + A_{33}) \ddot{\eta}_3(t) + B_{33} \dot{\eta}_3(t) + C_{33} \eta_3(t) - A_c P_0 \mu_u(t) = F_3^e(t) \quad (2.23)$$

$$(I_{55} + A_{55}) \ddot{\eta}_5(t) + B_{55} \dot{\eta}_5(t) + C_{55} \eta_5(t) - A_c P_0 x_{cp} \mu_u(t) = F_5^e(t). \quad (2.24)$$

Here, m is the mass of the vessel, A_{33} and A_{55} is the added mass coefficients in heave and pitch respectively, B_{33} and B_{55} is the wave radiation damping coefficients in heave and pitch, C_{33} and C_{55} is the hydrostatic restoring coefficients in heave and pitch, F_3^e and F_5^e are the hydrodynamic excitation forces in the heave and pitch degree of freedom.

Based on the cushion dynamics, equations of motion and the excitation forces an LTI state space

system can be written as:

$$\dot{\mathbf{x}}(t) = \mathbf{A}\mathbf{x}(t) + \mathbf{B}u(t) + \mathbf{E}\mathbf{v}(t), \quad (2.25)$$

where $\mathbf{x} = [\eta_3 \ \eta_5 \ \dot{\eta}_3 \ \dot{\eta}_5 \ \mu_u]^T$, $u = \Delta A_L$, $\mathbf{v} = [F_3^e \ F_5^e \ \dot{V}_0(t)]$, $\mathbf{A} \in \mathbb{R}^{5 \times 5}$, $\mathbf{B} \in \mathbb{R}^{5 \times 1}$ and $\mathbf{E} \in \mathbb{R}^{5 \times 3}$.

2.6.3 Stability Investigation

A proof of the Stability of the closed-loop system is found in Auestad et al. (2015). Here, by use of Lyapunov analysis, it is shown that the perturbed system is ultimately bounded. As the feedback gain parameter obtained from the adaptation described in Chapter 3 is kept positive, the results of the stability analysis performed by Auestad et al. (2015) is valid also for this control system.

Chapter 3

Adaptive Vertical Motion Control

The following chapter will contain a description of the adaptive controller developed for the SES. First with the feedback-controller, followed by a description of the adaptation scheme, exemplified by a simulation of controller initialization and transition to a higher sea state. An overview of the basic components of the adaptive control system is illustrated in Figure 3.1 and the relevant values used for the different parameters are presented in Appendix A.2. The objective of the adaptive controller is injecting dampening to the system in various operating conditions. The design is based on the current implementation of the feedback controller, however the adaptation scheme should render capabilities of adjusting the controller parameter automatically without operator intervention.

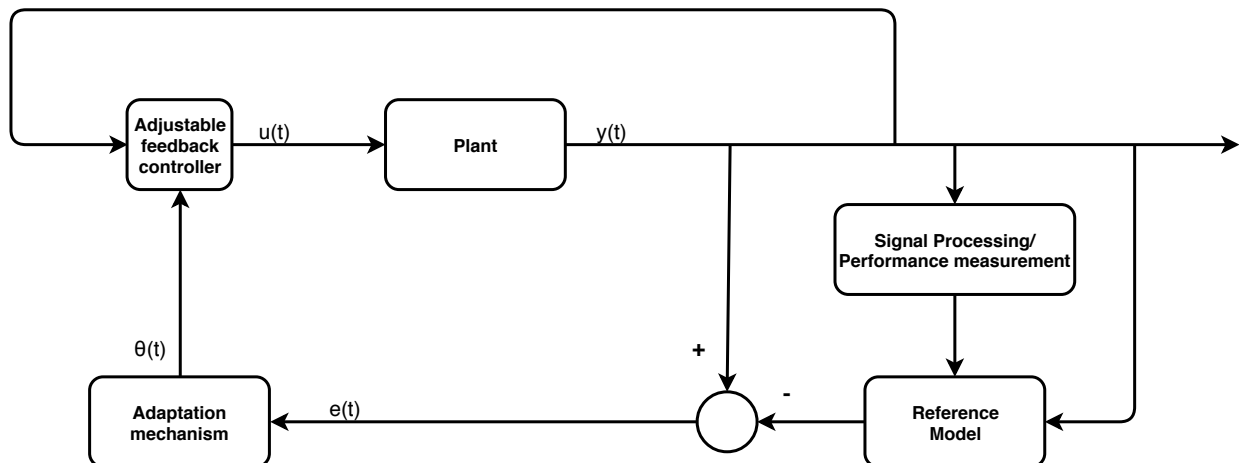


Figure 3.1: Basic overview of the adaptive control system

3.1 Feedback Controller

The feedback controller implemented follows a simple design. Auestad et al. (2015) provides a description and proof of stability for the closed-loop system. Through various simulations and testing of controllers of different structures, it was concluded that the following control law is able to inject the most dampening into the system, while maintaining a simple controller scheme with actuation proportional to the measured states. The following section describes the control system as implemented on the control plant model. However, the same control system was also applied to the SESSim model, simply by selecting controller inputs corresponding to the measurements from the same degrees of freedom in the two models.

The measurements $y(t)$ come from a numerically integrated, filtered accelerometer signal and is written:

$$y(t) = \mathbf{C}\mathbf{x}(t), \quad \mathbf{C} \in \mathbb{R}^{1 \times 5}. \quad (3.1)$$

The feedback control law can be expressed as:

$$u(t) = -\theta(t)y(t) = -\theta(t)\mathbf{C}\mathbf{x}(t), \quad \theta \in \mathbb{R}^+, \quad (3.2)$$

where θ is the controller feedback gain subject to adaptation. By adjusting the different coefficients in the matrix \mathbf{C} the ability to weight in contributions from different signals is obtained. Auestad et al. (2015) concludes that actuation proportional to the motion rates provides the most damping. Scaling the contributions from the measurements of heave and pitch provides the ability to prioritize damping in a specific point along the vessel longitudinally. This is in effect changing the relative phase between the changes in vent valve area and vessel motion. In this thesis, mainly damping in the center of gravity (COG) is emphasized, however simulations were also performed with prioritizing damping at the vessel bow, as well as a transition between the two during simulations.

The coefficients corresponding to heave and pitch rates, C_3 and C_4 are defined as:

$$C_3 = \frac{k_b + k_c}{m + A_{33}}, \quad C_4 = \frac{-k_c x_{c/b}}{I_{yy} + A_{55}}, \quad (3.3)$$

where $x_{c/b}$ is the longitudinal distance between the center of gravity and the bow, and k_b and k_c are parameters used to determine the location along the vessel where damping should be applied. For the simulations performed in this thesis, either k_b or k_c is set equal to 1 at a time. $k_b = 0$ and $k_c = 1$ injects most damping near the bow, while $k_b = 1$ and $k_c = 0$ injects most damping at the COG. This effect is apparent in Figure 3.2 and 3.3.

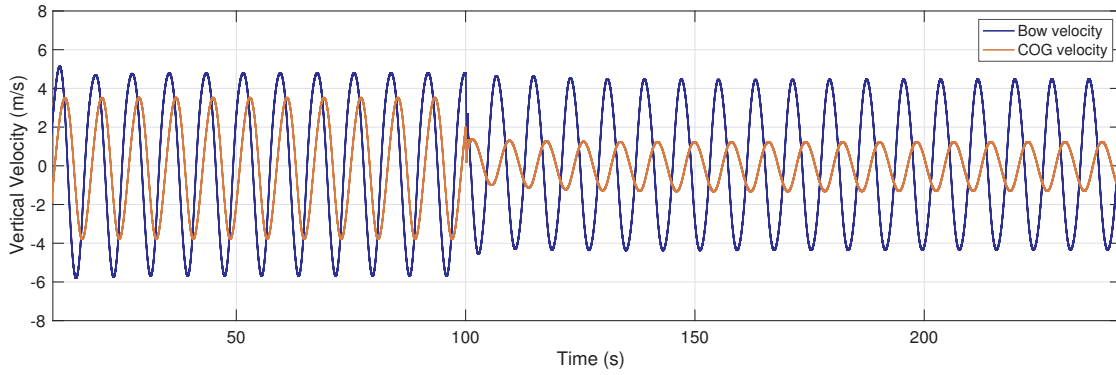


Figure 3.2: *Vertical velocity development with $k_b = 0$ and $k_c = 1$ - COG damping - Initiation at 100s*

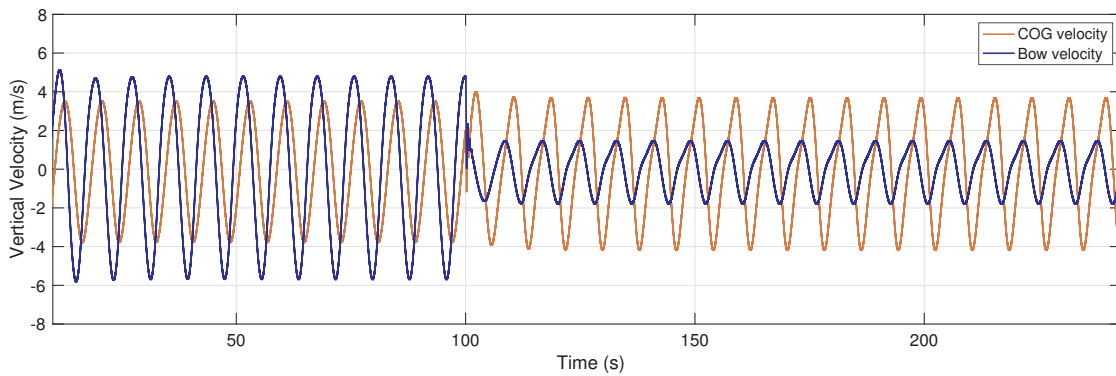


Figure 3.3: *Vertical velocity development with $k_b = 1$ and $k_c = 0$ - Bow damping - Initiation at 100s*

As the actuation of the vent valve louvers is proportional to the motion rates, and the fact that the motion rates are higher near the bow of the ship compared to the COG, a constant feedback gain parameter results in higher outputs for bow damping than COG damping. For large pitch motions relative to heave, if the gain parameter is kept constant, the controller output levels will be higher. This may cause problems for the actuators if the commanded vent valve leakage area jumps between the saturation limits of the controller output. A similar effect is seen if the gain parameter is kept constant as the level of motion rates increase. In the opposite case, when keeping a constant gain parameter for decreasing controller inputs, the system will not take full advantage of the potential damping. Being able to take advantage of the current damping capabilities of the system, without inducing vibrations or unnecessary wear on the actuators is the main motivation for applying an adaptation scheme to the feedback controller.

3.2 Parameter Adaptation

The purpose of the parameter adaptation, is altering the controller parameter, θ in such a way that the performance of the controller is acceptable for various disturbances inflicted on the system. Governing this process, is the controller *reference*. The reference signal, x_1, ref depicts the desired heave motion of the vessel. By comparing the reference signal to the measured motion, the reference error, e is obtained:

$$e(t) = x_1(t) - x_1, ref(t). \quad (3.4)$$

The controller parameter is set as a function of the reference and the current state of the system

$$\theta(t) = \int k_d(t)e(t)x_1(t)dt, \quad (3.5)$$

here, k_d represents a dynamic adaptation gain and is given by:

$$k_d(t) = \frac{k}{u_f(t)\ddot{z}_f(t)}, \quad (3.6)$$

where k is the adaptation gain, $u_f(t)$ is a filtered slowly varying representation of the controller output, and $\ddot{z}_f(t)$ is the similarly filtered representation of the vertical acceleration of the ship, based upon weighted and filtered accelerometer signals from the COG and bow of the ship. $\ddot{z}_f(t)$ is given by:

$$\ddot{z}_f(t) = C_1\ddot{\eta}_{3,f}(t) + C_2(\ddot{\eta}_{3,f}(t) - L_b\ddot{\eta}_{5,f}(t)), \quad (3.7)$$

where $\ddot{\eta}_{3,f}(t)$ and $\ddot{\eta}_{5,f}(t)$ is the filtered motion in the COG in the heave and pitch DOF and L_b is the longitudinal length between the COG and the bow. Use of accelerometer signals for heave motion estimation for a SES is treated in Auestad et al. (2013a)

The purpose of scaling the true adaptation gain in this manner is to allow for the controller parameter to experience changes of similar magnitude for a range of sea states. At low seas, the size of the measured state variable, and thus the size of the reference error are small relative to at higher seas. This leads to smaller contributions to the integral term in (3.5) which in turn results in a reduced adaptation rate at low seas and low levels of actuation. Correcting the adaptation gain relative to the filtered level of actuation increases the rate of which the adaptation scheme is able to respond when the controller is applied to the system. As the adaptation scheme seeks out a value for the controller parameter, the level of actuation increases which results in a decreased

ability to change after the initial response.

3.3 Controller Reference

A crucial component of the parameter adaptation scheme described in the previous section is the reference signal. Despite the purpose of the system being to minimize vertical motion, setting the reference signal equal to zero motion lies outside the capabilities of the current controller. The reference signal is instead chosen to be a signal in phase with the motion of the vessel, where the amplitude of the reference signal relative to the vessel motion reflects the current performance of the controller.

As the mentioned the controller sets the commanded vent valve opening proportional to the controller gain and the vertical velocity of the vessel. Consequently, in one sea-state, an increase in the controller gain leads to more rapid changes in the commanded vent valve opening, increasing the dampening of the vessel motion. However, as the gain increases the improvement in dampening fade, while potentially introducing unnecessary wear on the actuators and high-frequency vibrations.

However, the fact that an increase in controller gain leads to a decrease in vessel motion, forms the idea that for maximum performance, the controller gain should be increased as long as the change provides a further reduction in vertical accelerations without introducing vibrations from the actuators. This is the scheme behind how the tuning of controller parameters is performed manually in the current full-scale motion control system. For the purpose of establishing a controller reference, evaluating the change in vertical accelerations combined with the change in usage of the actuators is a way of automatically adjusting the controller parameter, coherent with the manual procedure.

As mentioned, the reference signal is a signal in phase with the motion of the vessel, where the amplitude of the reference relative to the amplitude of the motion directs how the controller parameter is altered. To set this amplitude, the following *cost-function* is introduced:

$$J = \mathbf{x}_f^T \mathbf{Q} \mathbf{x}_f + \beta u_f^2. \quad (3.8)$$

The constant matrix \mathbf{Q} functions as to weight in the contributions from the different states of the system combined in a single term and by this this providing a single measure of the degree of vessel motion. For the described feedback controller, \mathbf{Q} is defined as to mainly consider

vertical motions, as it is the main degree of freedom actuated by the system. For this thesis, adjustments to \mathbf{Q} are made according to whether damping is desired to be achieved mainly in the bow or COG. This is achieved by setting \mathbf{Q} using the same parameters k_b and k_c as the feedback controller (equation 3.3).

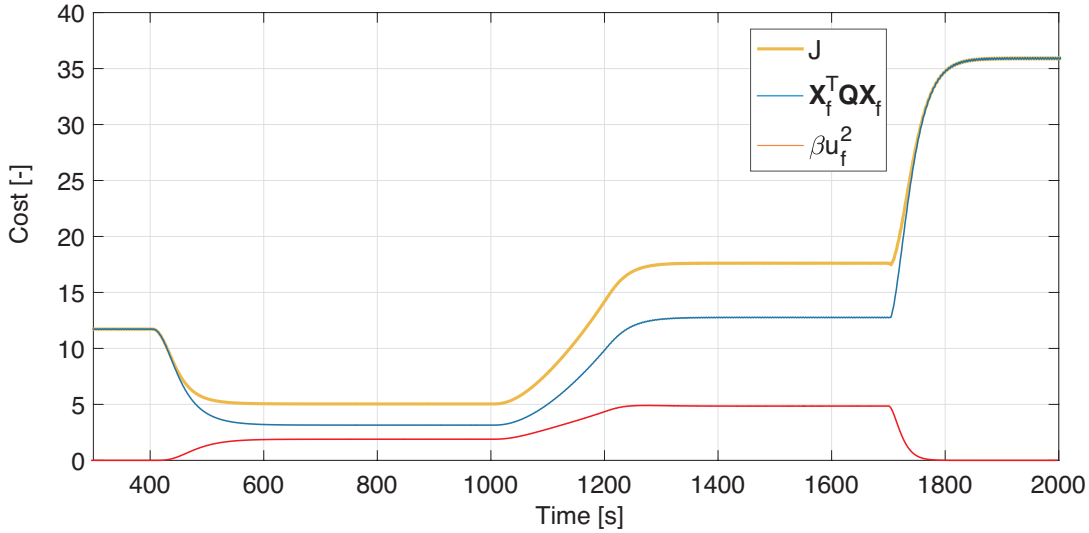


Figure 3.4: Cost function development during control activation (400 s), transition to a higher sea state (1000-1200 s) and deactivation (1700 s)

This equation incorporates both the degree of vessel motion and the level of actuation in a quadratic function. By seeking to minimize the value of this function, a balance between damping and actuation can be obtained. By tuning the matrix \mathbf{Q} and the parameter β , the point of where this balance exists may be adjusted. Emphasis on \mathbf{Q} relative to β results in seeking towards great usage of the actuators, maximizing the degree of dampening, while an opposite relation restricts usage of the actuators which limits the dampening capabilities. For the purpose of this adaptation scheme, the ratio is tuned such that a cost function minimum is found at an acceptable amount of dampening without saturating the controller outputs.

The reference signal x_{ref} is set by the following equation:

$$x_{ref}(t) = x(t) \left(1 + k_J \frac{dJ(t)}{dt} \right), \quad (3.9)$$

where k_J represents a gain parameter whose purpose is weighing in the contribution from the change in cost to the reference. As the change in cost approaches zero, the size of the reference signal approaches the size of the measurement signal (Figure 3.5).

To initialize the search towards the minimum of the cost function, a small perturbation is added

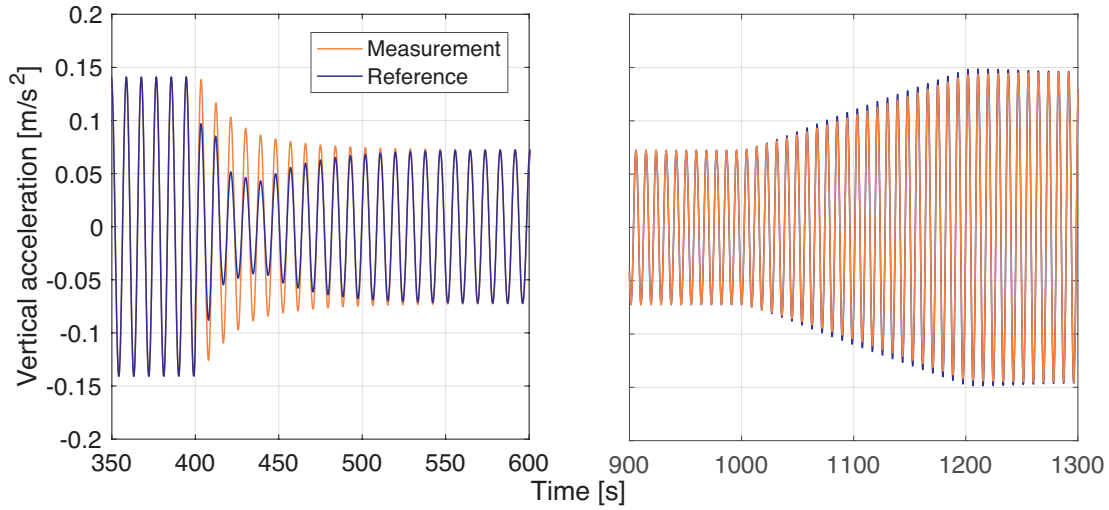


Figure 3.5: *Reference and measurement signal during initialization (Left) and transition to a higher sea state (Right)*

to the gain parameter θ . If an increase in the gain results in a lowering of the cost J , the adaptation scheme is designed such that the gain is further drawn in that direction, following the rate of change in J . Figure 3.6 displays the development of the gain parameter during the the previously depicted simulation. This also illustrates the effect of scaling the adaptation gain with the level of actuation, as the change in gain is much larger at the initial start-up compared to at the transition from one sea-state to another despite the change in value of the cost function being larger in the transition phase (Figure 3.4).

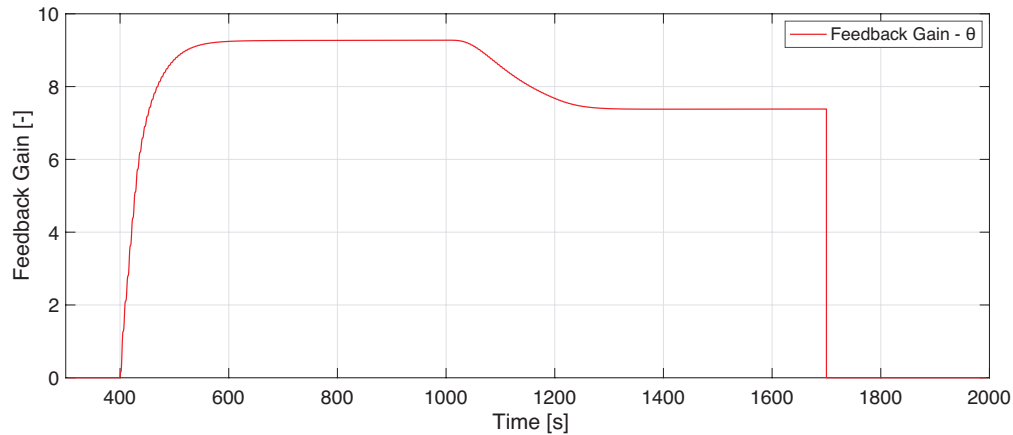


Figure 3.6: *Gain development during initialization, transition to a higher sea state and deactivation*

3.4 Signal Processing

As the adaptation scheme is strongly dependent of variations of the sea-state over time, a way of distinguishing between low-frequency changes in the wave forces and the *wave-frequency* components is required. Several alternatives for acquiring some measure of these variations over time were tested.

Following Fossen (2011) a Butterworth low pass filter is introduced for wave filtering. This type of filter is designed to have the property of rejecting frequencies in the stopband while maintaining a flat *frequency response* in the passband. This means changes to the low frequency forces in the passband frequency range are treated close to equally. In the areas of operation for the SES-type described in this thesis, The dominating wave frequencies typically encountered lie in the range of $0.05Hz$ to $0.2Hz$, corresponding to wave-periods between $5s$ and $20s$. Low-frequency variations to the wave forces however, arise at much larger time-scales. The transition duration is exaggerated in the simulation depicted above. Still, for the initial response of the adaptation scheme the cutoff frequency ω_f should be large enough as to allow an acceptably fast response when the system is activated. The Butterworth filter is a way of designing a higher order low-pass filter, where a higher order allows for a sharper distinction between the preserved and attenuated frequencies. The transfer function for the second order Butterworth filter is defined by:

$$h(s) = \frac{\omega_f^2}{s^2 + 2\zeta\omega_f s + \omega_f^2}, \quad \zeta = \sin\left(\frac{\pi}{4}\right). \quad (3.10)$$

As the purpose of the filtering is capturing the magnitude of the average vessel motion and the actuator usage over time, some fluctuations in the filtered output is acceptable and as the resulting reference error is integrated in the parameter adaptation, these effects average over time for one sea state. Additionally, a relatively small change in the resulting controller parameter has little impact on the resulting dampening capabilities for the system, thus some fluctuations in the filtered output is allowed at the gain of reduced phase lag.

Chapter 4

Results

This chapter will present the results obtained through vessel simulations performed with the developed controller applied to the two described models. The results of each simulation will be presented using the time-series plots of the quantities deemed relevant to describe the behavior of the system, in addition to spectral power density plots for the simulations done at irregular seas. Following the resulting plots of each simulation will be a short description of the results and a discussion around the controller behavior for the current case with comparisons to other cases when relevant.

The environmental conditions used in the simulations performed are selected to display the adaptive behavior of the controller for different sea states. This is done by using regular waves of varying amplitude and frequency, irregular waves drawn from different wave-spectra, and by alternating the longitudinal location of where damping is injected between the center of gravity and the vessel bow.

Simulations with transitions between sea states or between bow and COG damping are done in pairs. Meaning for example that if a simulation is done where the surface elevation time-series move from a low sea state to a higher sea state, the same simulation is repeated with the wave elevation time series applied in reverse.

Note that the simulations are done on SES vessel models which emulate dynamics similar to those of the WAVECRAFT™, but not identical in terms of performance.

4.1 Overview of Simulations

The simulation cases selected are chosen to capture the behavior of the adaptive controller in various scenarios. The tuning parameters for the adaptive controller are kept constant for comparable tests, while some changes had to be made to the parameters when changing from the control plant model to the SESSim model or from regular to irregular waves. This has to be taken into consideration if comparing the magnitude of the time-series quantities from different simulations.

The different simulations will be presented as follows:

- Initial response and changing sea state in regular waves using the control plant model.
- Initial response and changing sea state in irregular waves using the control plant model.
- Initial response in irregular waves using the SESSim model.
- Initial response and changing point of damping between COG and bow in regular waves using the SESSim model.

4.2 CPM Response in Regular Waves and Changing Sea State

This section will display the results obtained with simulations done with the control plant model in regular waves. The objective in these simulations are decreasing the vertical motion of the vessel center of gravity.

The presented plots depict the relevant quantities required to describe the initial response when control is applied, and the ability to transition between sea states of different amplitudes. The selected sea states for the tests are: $H_s = 0.8\text{ m}$ with $T_s = 7\text{ s}$, $H_s = 1.4\text{ m}$ with $T_s = 7.5\text{ s}$ and $H_s = 2.0\text{ m}$ with $T_s = 8.8\text{ s}$. Frequencies are kept relatively close due to limitations found in the range of frequencies of the control plant model.

Presented here are the results from transitioning between $H_s 1.4\text{ m}$ and $H_s 2.0\text{ m}$. Simulations for a transition between $H_s 0.8\text{ m}$ and $H_s 1.4\text{ m}$ yielded similar results which are found in Appendix B.

4.2.1 Initialization and Transition from H_s 1.4 to 2 m

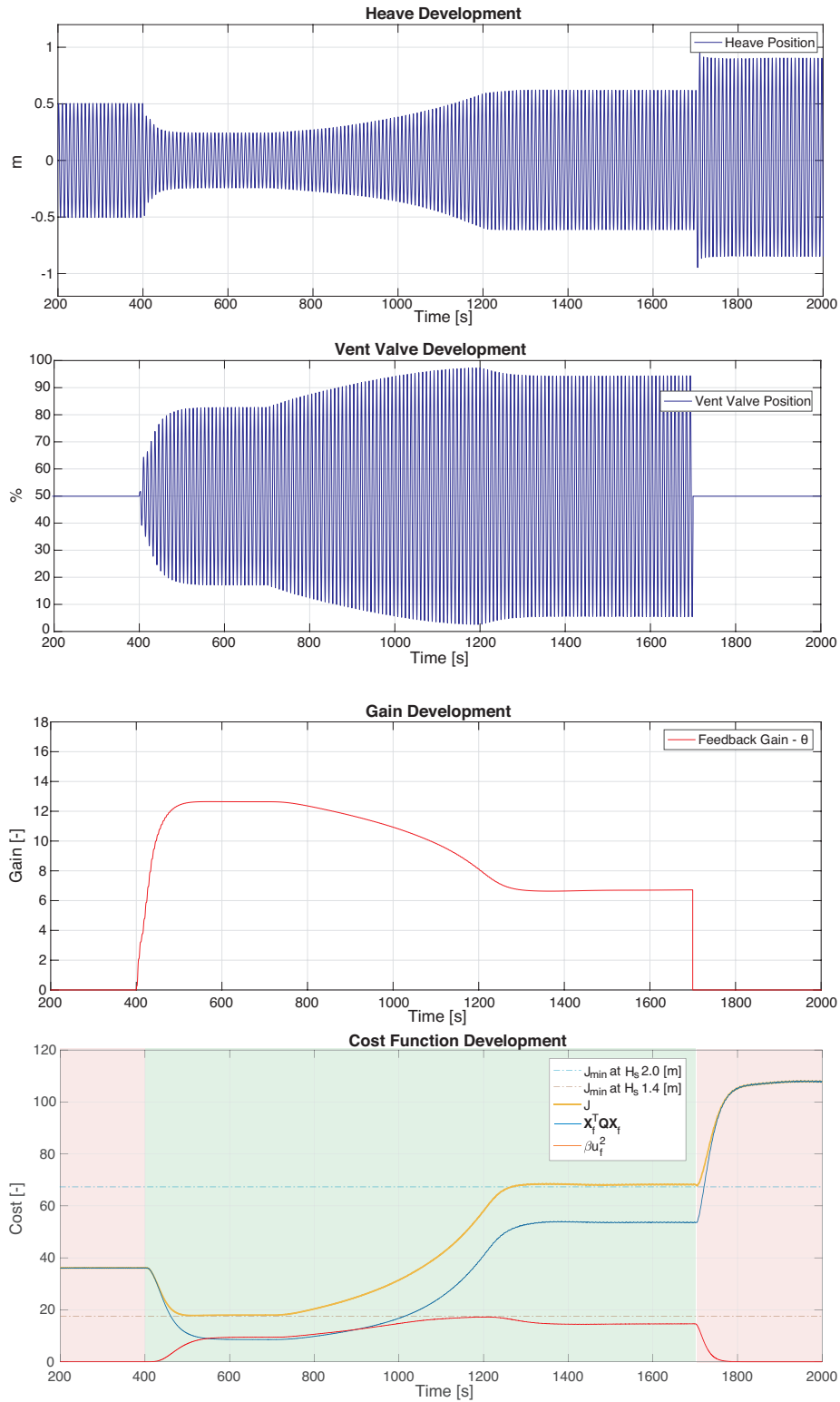


Figure 4.1: Simulation results for $H_s = 1.4$ m, $T_s = 7.5$ s to $H_s = 2$ m, $T_s = 8.8$ s

In this simulation, control is applied at 400 s. The transition of sea state starts at 700 s and lasts until 1300 s.

The initial gain ramp-up at $H_s = 1.4$ m is smooth, and starts flattening out as the level of actuation increases. Once the increase in actuation and decrease in vessel motion cancels each other out the gain parameter stabilizes around a value of 12, which corresponds to the vent valve actuators oscillating between approximately 60% of their limits for this sea state. The controller is disabled after 1700 s to visualize the motion with no injected damping. The activation and deactivation of the control system is also indicated by the change in color overlay on the plot of the cost function.

As the size of the waves increase, both the degree vessel motion and the level of actuation rise as depicted by the cost function. To compensate, the gain is lowered until the transition is over and restabilizes at a value of around 7, corresponding to about 90% usage of the ventilation valves.

The minimum in the total cost displayed in the plot of cost function has been found by running a simulation for the same two sea states and letting the gain parameter slowly ramp up from zero. The result is a depiction of the cost as a function of gain (Figure 4.2), where the function minimum represents the target gain for the current controller configuration and sea state.

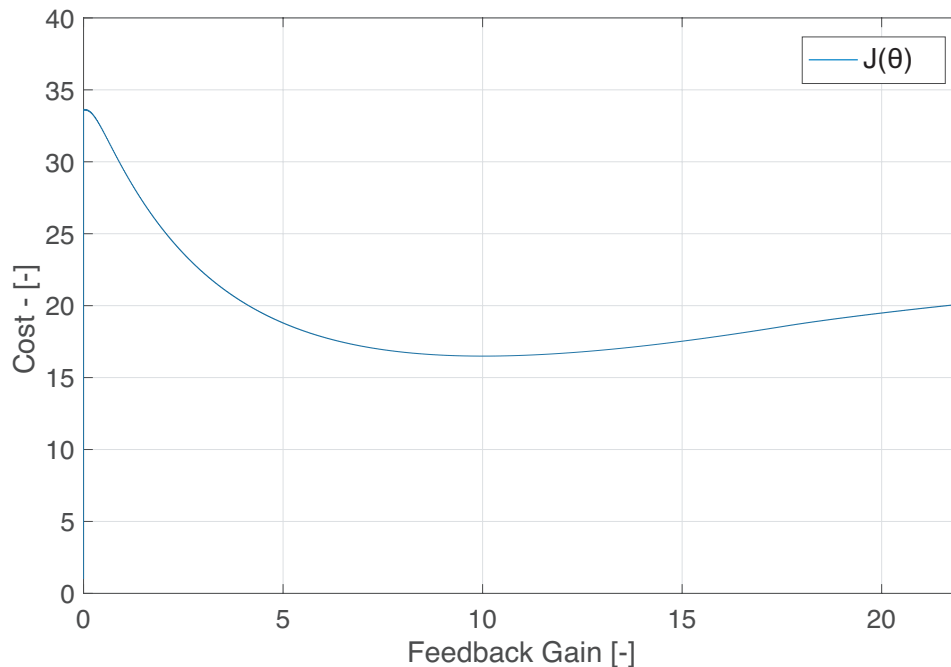


Figure 4.2: Cost function value for varying feedback gain at $H_s = 1.4$ m, $T_s = 7.5$ s

4.2.2 Initialization and Transition from H_s 2 to 1.4 m

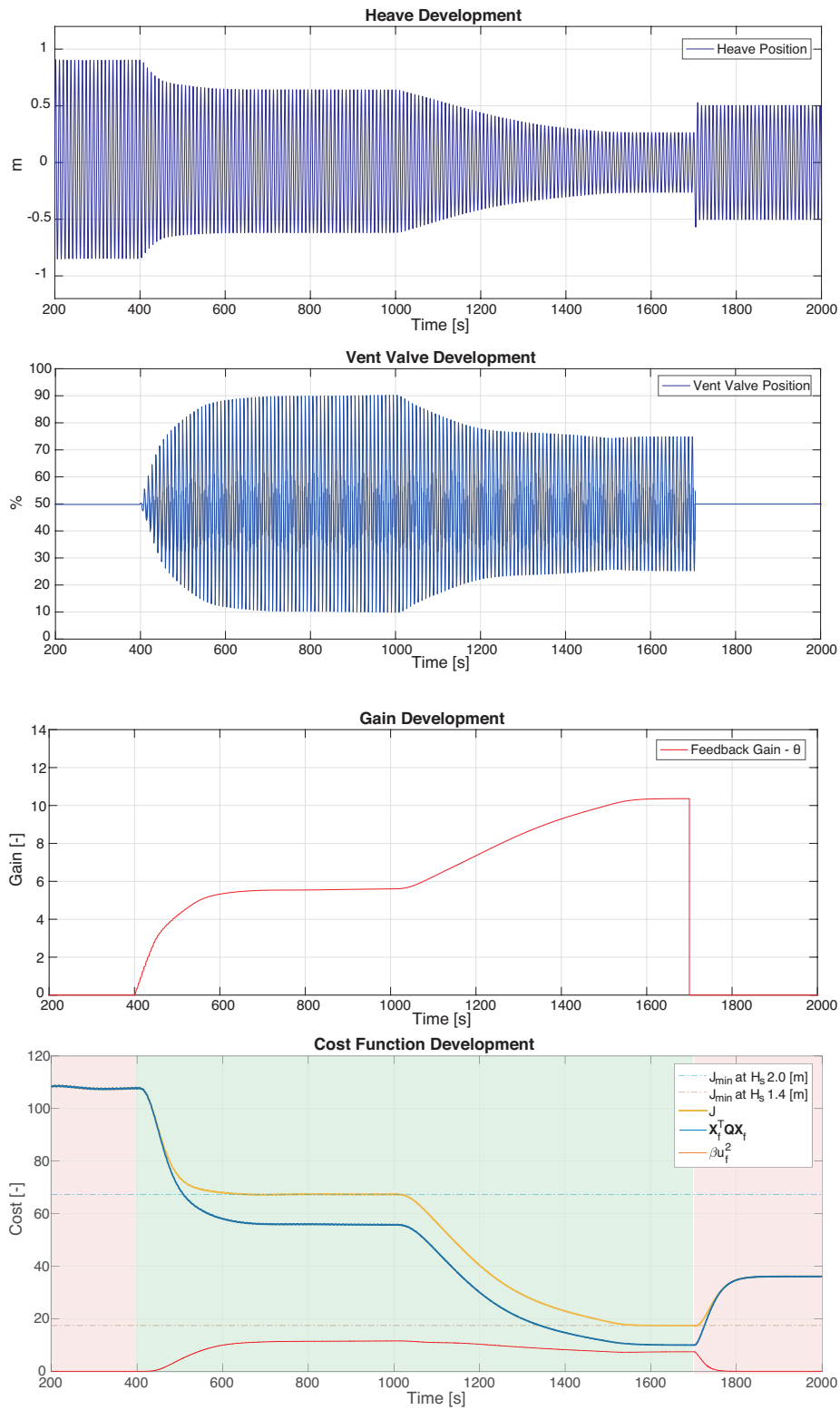


Figure 4.3: Simulation results for $H_s = 2\text{ m}$, $T_s = 8.8\text{ s}$ to $H_s = 1.4\text{ m}$, $T_s = 7.5\text{ s}$

In this simulation control, is applied at 400 s and disabled at 1700 s. The transition of sea state starts at 1000 s and lasts until 1600 s. The initial response of the feedback gain at $H_s = 2\text{ m}$ is as desired; ramping up and stabilizing at a value around 7 which leads to the actuators not being saturated. However, the transient period before stabilizing is longer compared to the response at a lower amplitude. This is explained in part by the fact that the relative damping capabilities are lower at higher seas due to limitations in the actuators. At the same time, as mentioned in section 3.2, the rate of adaptation is lowered at higher seas to avoid the gain becoming too large and reaching saturation of the actuators. As the vessel motions become smaller after 1000 s, the gain is heightened to compensate for some of the decrease in actuator usage.

It is also observed that the resulting gain parameter at one sea state is not exactly equal for the simulations depicted here and in section 4.2.1. As visualized by Figure 4.2 and 4.4, the cost functions are convex in the relevant region of gain parameters, meaning there exists a distinct minimum for where the lowest cost-value may be obtained. However, for a given gain parameter value, without a sufficient disturbing perturbation of the inputs, the adaptation scheme halts. This means that as the ratio between the change in value of the cost function and change in level of actuator usage becomes too small, the rate of adaptation of the controller diminishes. The distinctiveness of the minimum in the cost function minimum determines the extent of this effect. Should the system be persistently excited, as is the case for irregular waves where the value of the cost function has a sufficient level of continuous variation, the search for the cost function minimum persists.

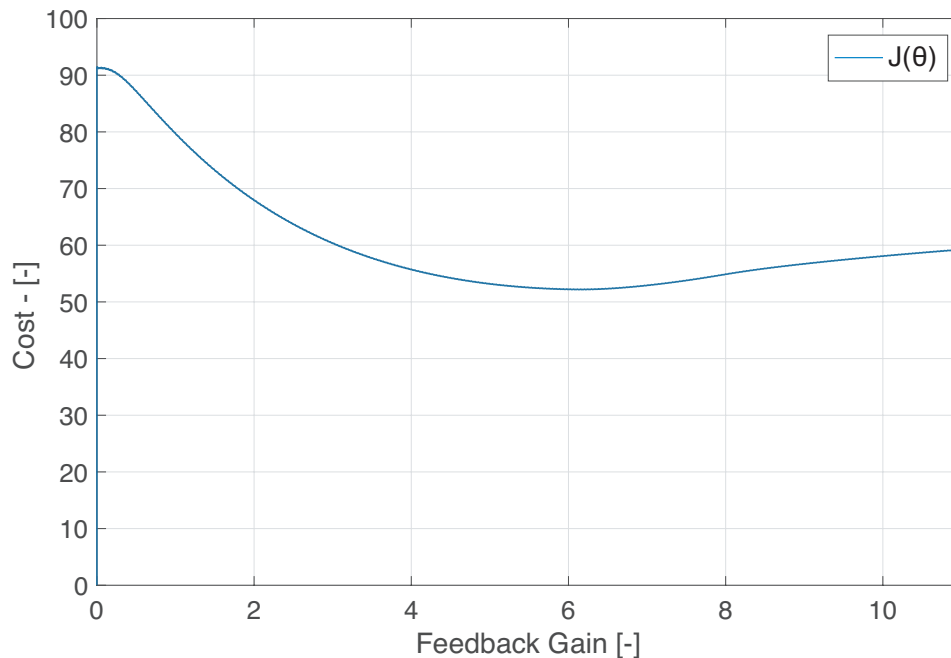


Figure 4.4: Cost function value for varying feedback gain at $H_s = 2\text{ m}$, $T_s = 8.8\text{ s}$

4.3 CPM Response in Irregular Waves and Changing Sea State

The following section will display the results from simulations on the control plant model in irregular waves. The objective of control is similar to the previous section: decreasing the vertical motion in the center of gravity. The purpose of these simulations is to investigate the applicability of the developed controller to irregular waves and its implications.

The wave elevation time-series are drawn from the Jonswap spectrum as defined in equation 2.15. The selected sea states are $H_s = 1\text{ m}$ with $\omega_p = 0.9\frac{\text{rad}}{\text{s}}$ and $H_s = 1.5\text{ m}$ with $\omega_p = 0.8\frac{\text{rad}}{\text{s}}$ with their respective spectra illustrated in Figure 4.5. These simulations are run for 3000s which is longer than for the cases with regular waves. This is due to how the existence of multiple frequencies in the irregular waves requires the low pass Butterworth filter to be tuned with a lower cutoff frequency, to provide usable inputs to the controller. This, in turn, causes added phase lag which reduces the responsiveness of the controller compared to the regular wave case.

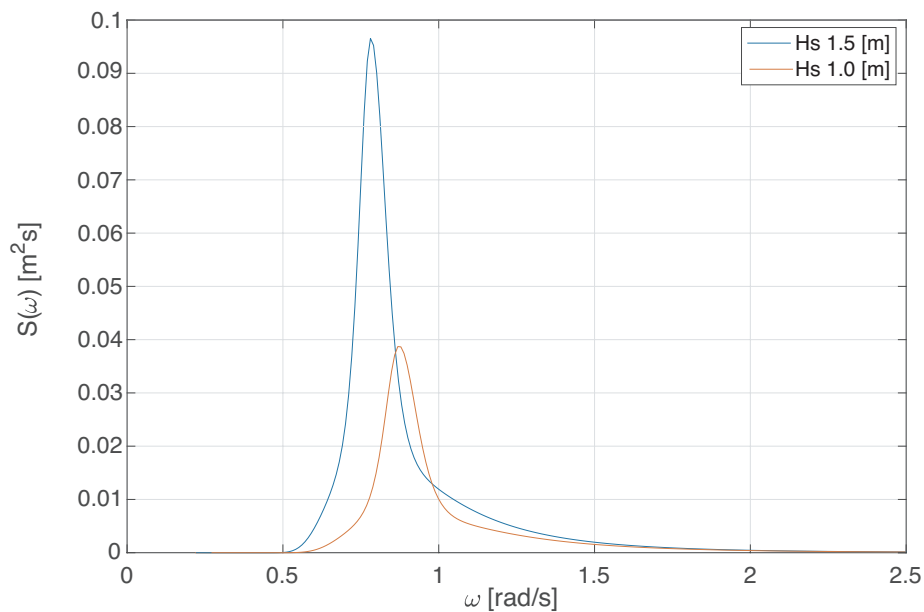


Figure 4.5: Jonswap wave spectra for $H_s = 1.5\text{ m}$ and $H_s = 1\text{ m}$ used in control plant model

4.3.1 Initialization and Transition from H_s 1 to 1.5 m

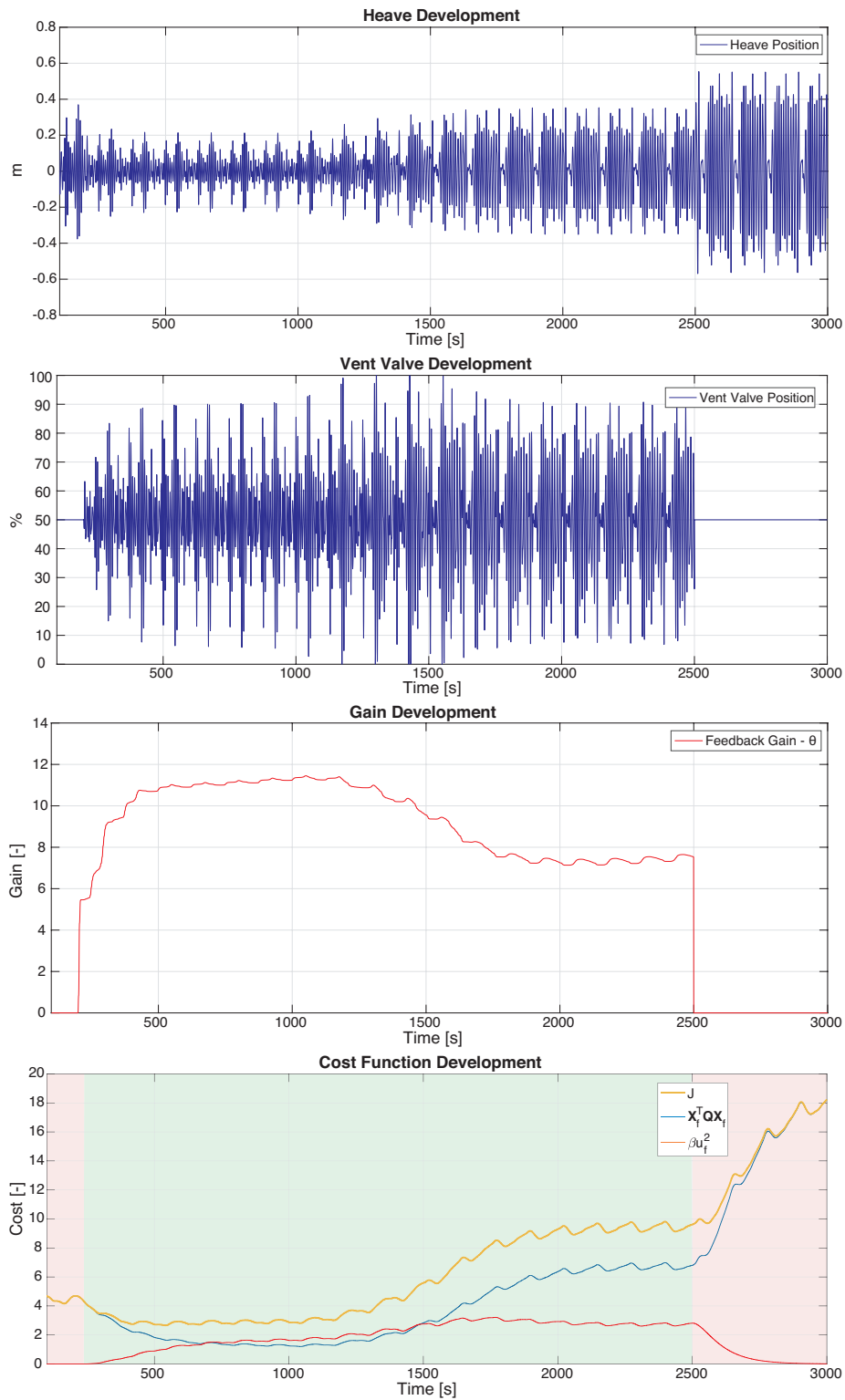


Figure 4.6: Simulation results for $H_s = 1 \text{ m}$, $\omega_p = 0.9 \frac{\text{rad}}{\text{s}}$ to $H_s = 1.5 \text{ m}$, $\omega_p = 0.8 \frac{\text{rad}}{\text{s}}$

In this simulation, control is applied at 200 s, the transition of sea state begins at 1200 s and lasts until 1800 s. The controller is disabled after 2500 s. The initial response is an increase in gain before stabilizing at a value of about 11 which results in a dampening of the vertical vessel motion. Once the vessel motion increase, the actuator usage follows and the gain is reduced.

These results illustrate some of the challenges faced with the chosen approach to an adaptive controller. The scheme is dependant on the input of the slowly varying level of motion and actuator usage, which is obtained by filtering the wave-frequency accelerometer and louver signals. The variations observed in the gain are due to how the filtered output contains some fluctuations. These fluctuations could be decreased by applying a lower cutoff frequency or an alternative form of filtering. Still, this could impose more delays in the adaptation and initial response which is not desired. The observed fluctuations in the feedback gain are deemed acceptable, as these variations have a small impact on the actuator usage and the overall motion damping capabilities of the system.

Figure 4.7 depicts the power spectral density (PSD) of the heave position, recorded between 500 and 1000 s when $H_s = 1$ m and the feedback gain is relatively steady. This is compared to the results obtained in a simulation done with the same wave elevation series and no control applied. As the integral of the PSD represents kinetic energy, it is clear that the damping injected by the system is able to dissipate a substantial part of the kinetic energy in the system. By numerical integration of the PSD it was found that the size of the integral in the controlled case was 20% of the size of the integral in the uncontrolled case.

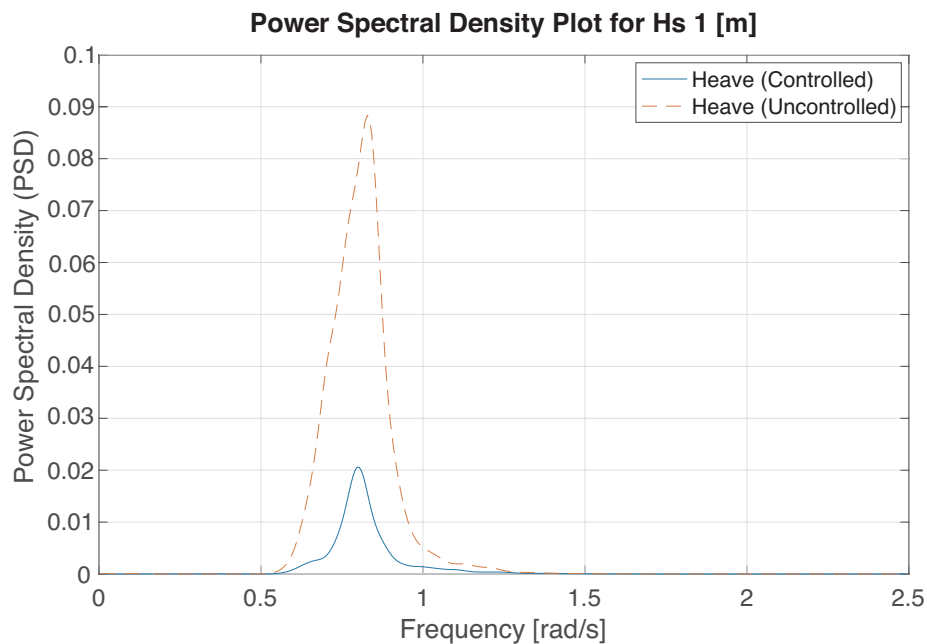


Figure 4.7: Power spectral density plot for Hs 1 m - Control Plant Model

4.3.2 Initialization and Transition from H_s 1.5 to 1 m

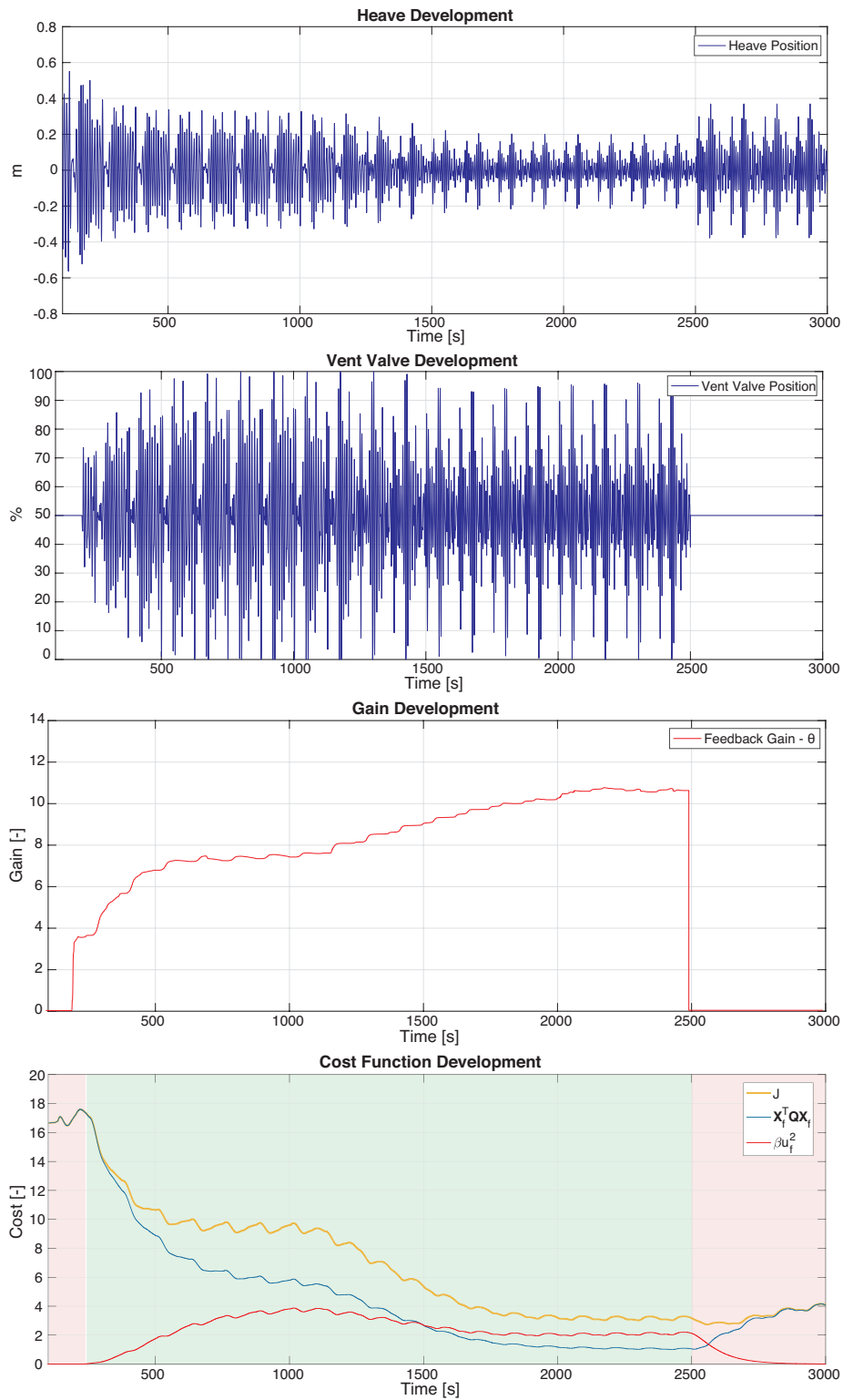


Figure 4.8: Simulation results for $H_s = 1.5 \text{ m}$, $\omega_p = 0.8 \frac{\text{rad}}{\text{s}}$ to $H_s = 1 \text{ m}$, $\omega_p = 0.9 \frac{\text{rad}}{\text{s}}$

In this simulation, control is applied at 200 s, the transition of sea state begins at 1200 s and lasts until 1800 s. The initial response is an increase in feedback gain before stabilizing after about 300 s. As the vertical motions decrease during the transition, the gain is increased to maintain some usage of the actuators.

Similar to in the case of regular waves, it is clear that the time it takes for the gain to stabilize is longer for a higher sea state. Both in this case and the one previously mentioned in Section 4.3.1 there is an abrupt initial step in the feedback gain upon initiation, which is due to how an initial perturbation is added to the controller reference when the adaptation is initiated as mentioned in Section 3.3. For the simulations done with irregular waves, the size of this perturbation was increased compared to when using regular waves. This was done to ensure that the adaptation scheme would not be halted due to a sudden increase in the filtered controller inputs. This is in effect "forcing" the resulting gain in one direction initially, which was found to be an advantage when the filtered inputs are delayed and experience some fluctuations due to the irregular waves. Figure 4.9 depicts the PSD of the heave position recorded between 500 and 1000 s when $H_s = 1.5$ m and compares it to a simulation done without applied control. It is evident that the control system is able to dissipate kinetic energy from the system. Compared to the corresponding plot from $H_s = 1$ m depicted in Figure 4.7 the degree of dampening is similar. Integration of the resulting PSD reveals that the size of the integral in the controlled case is 17% of the size in the uncontrolled case. Compared to the same results in Section 4.3.1, the relative degree of dampening is larger at the higher sea state.

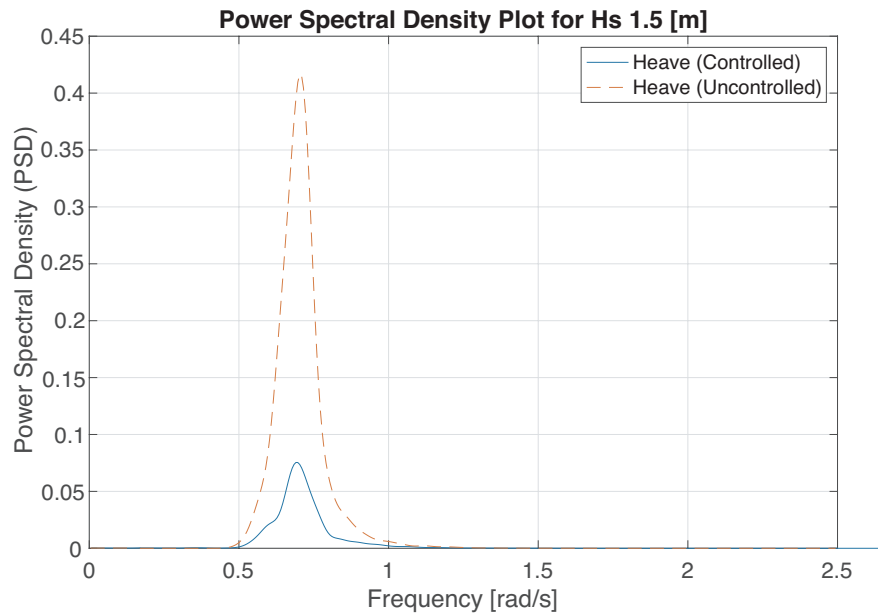


Figure 4.9: Power spectral density plot for Hs 1.5 m - Control Plant Model

4.4 SESSim Response in Irregular Waves

This section will present the results from simulations done on the SESSim process plant model. This is done to verify the results obtained in the control plant model and to investigate the controller behavior in a model with a wider range of implemented dynamics.

The SESSim includes a non-linear cushion model, fluid memory effects, non-linear damping, coupling dynamics and other effects in 6 DOF, which is not accounted for in the simplified control plant model. This means that the results obtained lie closer to what may be observed on a full-scale vessel. The increased degree of complexity in this model however, makes running numerous simulations more time-consuming than in the control plant model.

The simulations presented here depict the initial response after control is initiated. The sea states tested are $H_s = 1\text{ m}$ with $\omega_p = 0.8 \frac{\text{rad}}{\text{s}}$ and $H_s = 1.5$ with $\omega_p = 0.9 \frac{\text{rad}}{\text{s}}$. These are similar sea states to those applied to the control plant model in Section 4.3.1 and 4.3.2 and the spectra for the wave elevation time-series generated by the SESSim model are depicted in Figure 4.10.

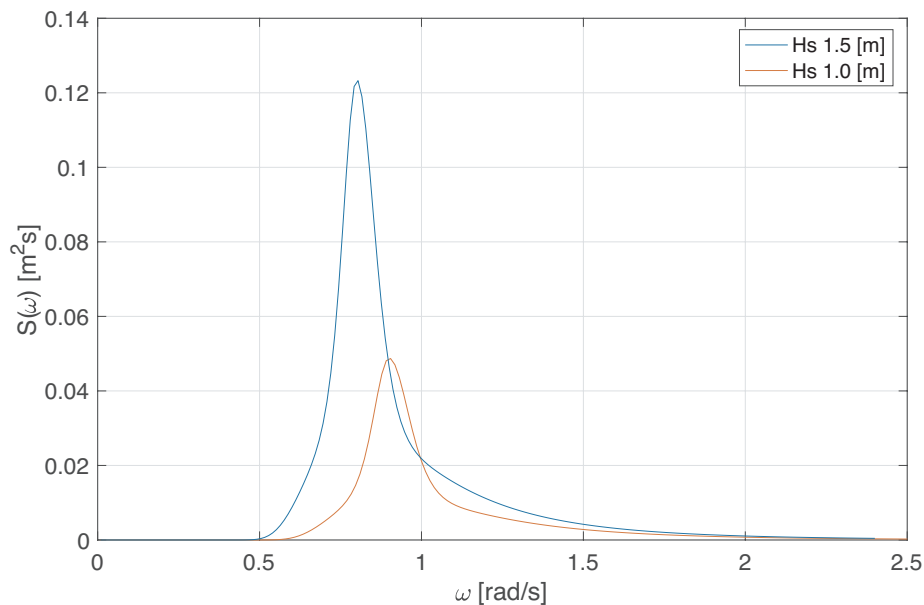


Figure 4.10: Jonswap wave spectra for $H_s = 1.5\text{ m}$ and $H_s = 1\text{ m}$ used in SESSim model

4.4.1 Initialization at H_s 1 m

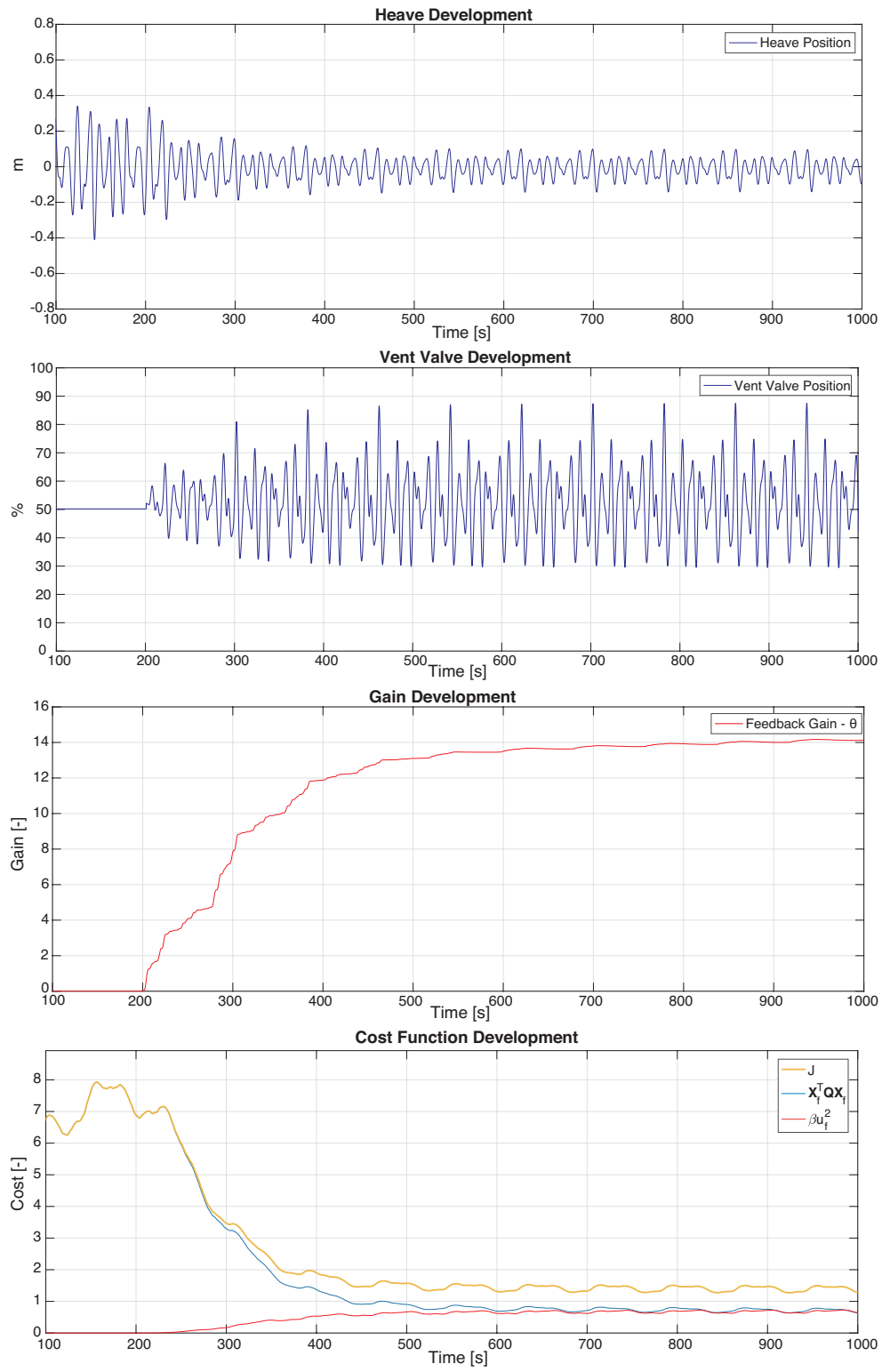


Figure 4.11: Simulation results for $H_s = 1$ m, $\omega_p = 0.9 \frac{rad}{s}$

In this simulation, control is applied after 200 s, the gain parameter ramps up and stabilizes around a value of 14 after 400 s and a reduction in vertical motion is observed.

When comparing this initial response to the ones found for similar waves in the control plant model in Section 4.3.1, similarities in both the vessel response and the development of the adaptation gain are found. Figure 4.12 depicts the power spectral density recorded between 500 and 1000 s and a similar recording in the uncontrolled case. By integrating and comparing the PSD it is found that the size of the integral in the controlled case is 13% of the corresponding integral in the uncontrolled case. This reduction is larger than the one found using the control plant model, despite that the time-series of the vent valves show similar if not a smaller degree of actuator usage in the SESSim model.

A suggestion as to why the SESSim model experience a larger degree of damping than the simplified model can be found in the linear pressure model. The *orifice* coefficient, c_n , which is multiplied by the change in leakage area ΔA_L in Equation 2.22, is an assumption made to account for flow losses due to the vent valve duct shape. Sørensen and Egeland (1995) estimates this value at 0.61 which is used in the control plant model. Auestad et al. (2015) however suggests that this value is too conservative when comparing results to full-scale tests. A decrease in the orifice coefficient is in practice restraining the actuators capabilities of changing the cushion pressure, which may be an explanation to the observed larger degree of damping in the SESSim results.

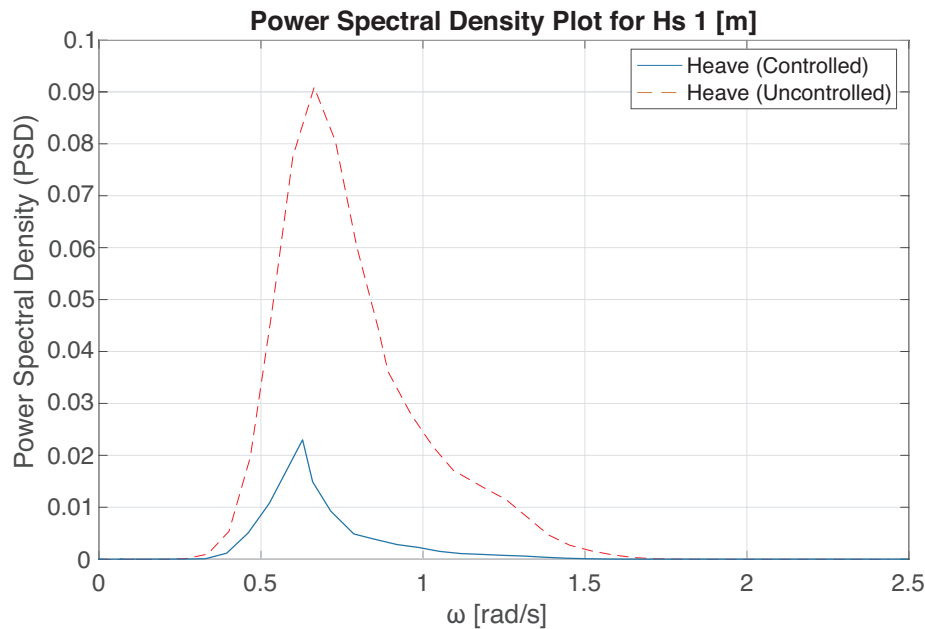


Figure 4.12: Power spectral density plot for Hs 1 m - SESSim model

4.4.2 Initialization at $H_s = 1.5\text{ m}$

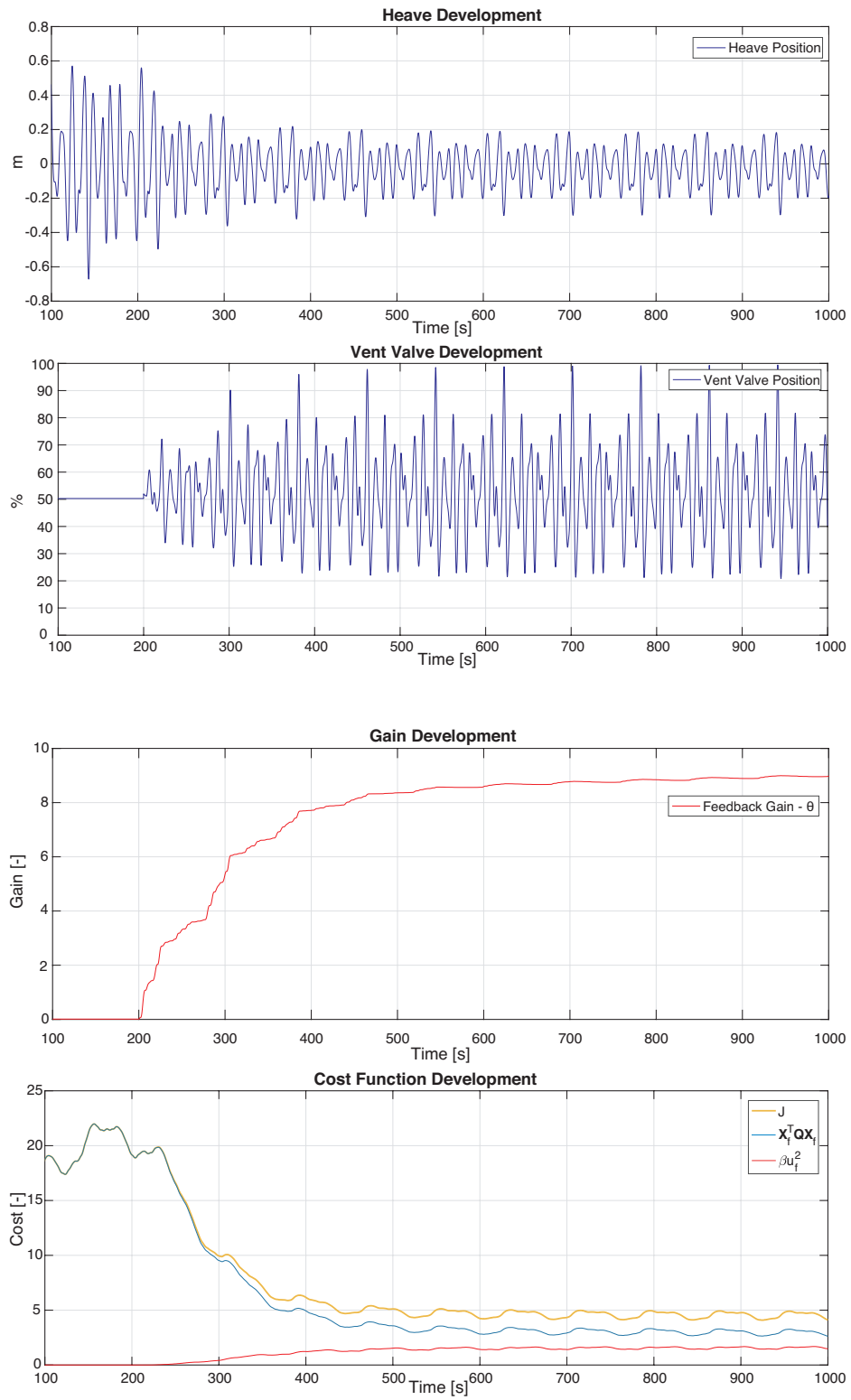


Figure 4.13: Simulation results for $H_s = 1.5\text{ m}$, $\omega_p = 0.8 \frac{\text{rad}}{\text{s}}$

In this simulation, control is applied after 200 s. The initial response is an increase in gain before settling around a value of about 9 at 500 s.

As in the simulations for the control plant model, the resulting feedback gain is lower than the one obtained at a higher sea state (Section 4.4.1) which is desired. The PSD plot depicted in Figure 4.14 displays a similar degree of reduction in power spectral density to the ones found in previous simulations done for irregular waves. When integrating and comparing the controlled and uncontrolled case, it is found that the size of the integral in the controlled case is 12% of that in the uncontrolled case. This is close to the value found at $H_s = 1\text{ m}$ from Section 4.4.1, albeit slightly evident of an increased ability of injecting damping at the higher sea state which is coherent with the results from the control plant model.

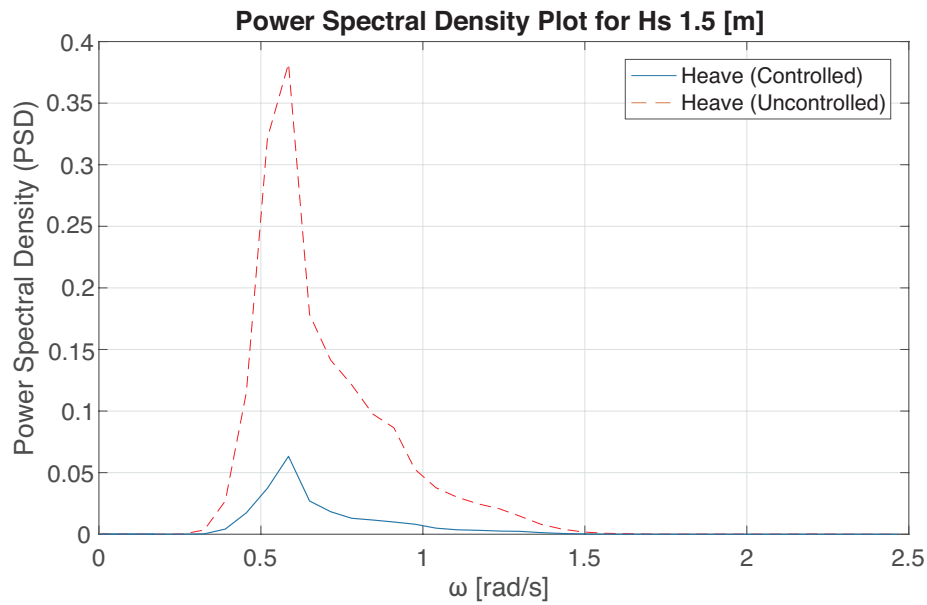


Figure 4.14: Power spectral density plot for Hs 1.5 m - SESSim model

4.5 Response in Regular Waves - COG and Bow Damping

The following section will present the results obtained when running simulations where the longitudinal point of where damping is injected is changed between the bow and center of gravity (COG). Reducing vertical motions in the bow for boarding purposes is one of the key features of the Wavecraft™ which means that having an adaptive controller which is able to handle both COG and bow damping is an advantage. As the feedback control law (Equation 3.2) is the same for both forms of damping, the previously presented results are valid in both cases. However, transitioning between COG and bow damping has a few implications for the adaptive scheme.

Equation 3.3 states that the magnitude of the vertical motion of the bow is always equal to or greater than the motion of the COG, where the difference in magnitude is dependent on the *pitch angle*. This implies that vertical velocities are greater at the bow, which means that the controller will command greater actuator usage for a constant feedback gain when damping bow motions compared to COG motions. For the controller, this is analogous to a change in sea state as previously presented. This means that when transitioning from COG to bow damping, the adaptive controller should reduce the gain and vice versa.

For these simulations, the vessel is exposed to regular waves and the SESSim model is used. Using the SESSim model in these simulations is an advantage as it has implemented coupling effects in heave and pitch, which are essential when investigating the motion of the bow.

The sea state selected is $H_s = 1.5 \text{ m}$ with $T_s = 6 \text{ s}$. These are rather *steep waves*, meaning they have a rather short period relative to amplitude, which is a choice made as means of inducing large pitch motions relative to heave.

4.5.1 Initialization and Transition from COG to Bow Damping

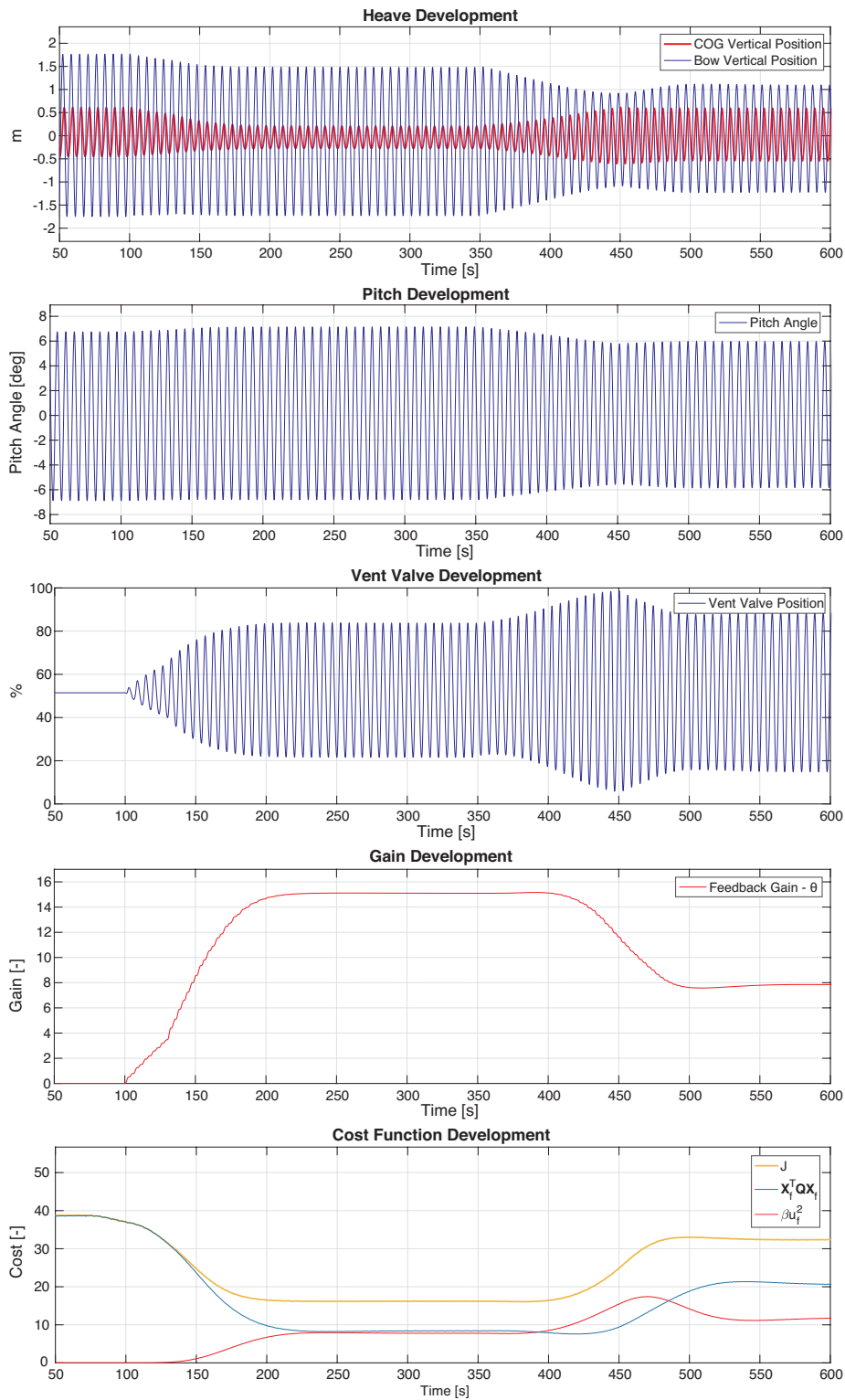


Figure 4.15: Simulation results for $H_s = 1.5 m$, $T_s = 6 s$ - COG to Bow Damping

In this simulation, control is applied at 100 s with damping injected at the COG of the vessel. At 350 s damping is directed towards the bow and at 500 s the transition is complete with all the damping being injected at the bow.

When control is applied, the feedback gain ramps up and stabilizes around a value of 15 after about 200 s. A reduction in the COG motion and a smaller reduction in the bow motion is observed. The pitching motion remains approximately the same until damping is transitioned towards the bow. During the transition, there is a peak in the actuator usage, as the controller is receiving inputs from both the vertical velocity at the bow and at the COG. The increase in actuator usage leads to a reduction in the feedback gain. After the transition, the controller is able to reduce the vertical motions of the bow, at the cost of increased COG motions.

When comparing these results to the case of transitioning to a higher sea state in regular waves as described in Section 4.2.1, similarities in the behavior of the adaptive controller are found. In both cases, the controller is able to adapt to the increased actuator usage by reducing the feedback gain.

4.5.2 Initialization and Transition from Bow to COG Damping

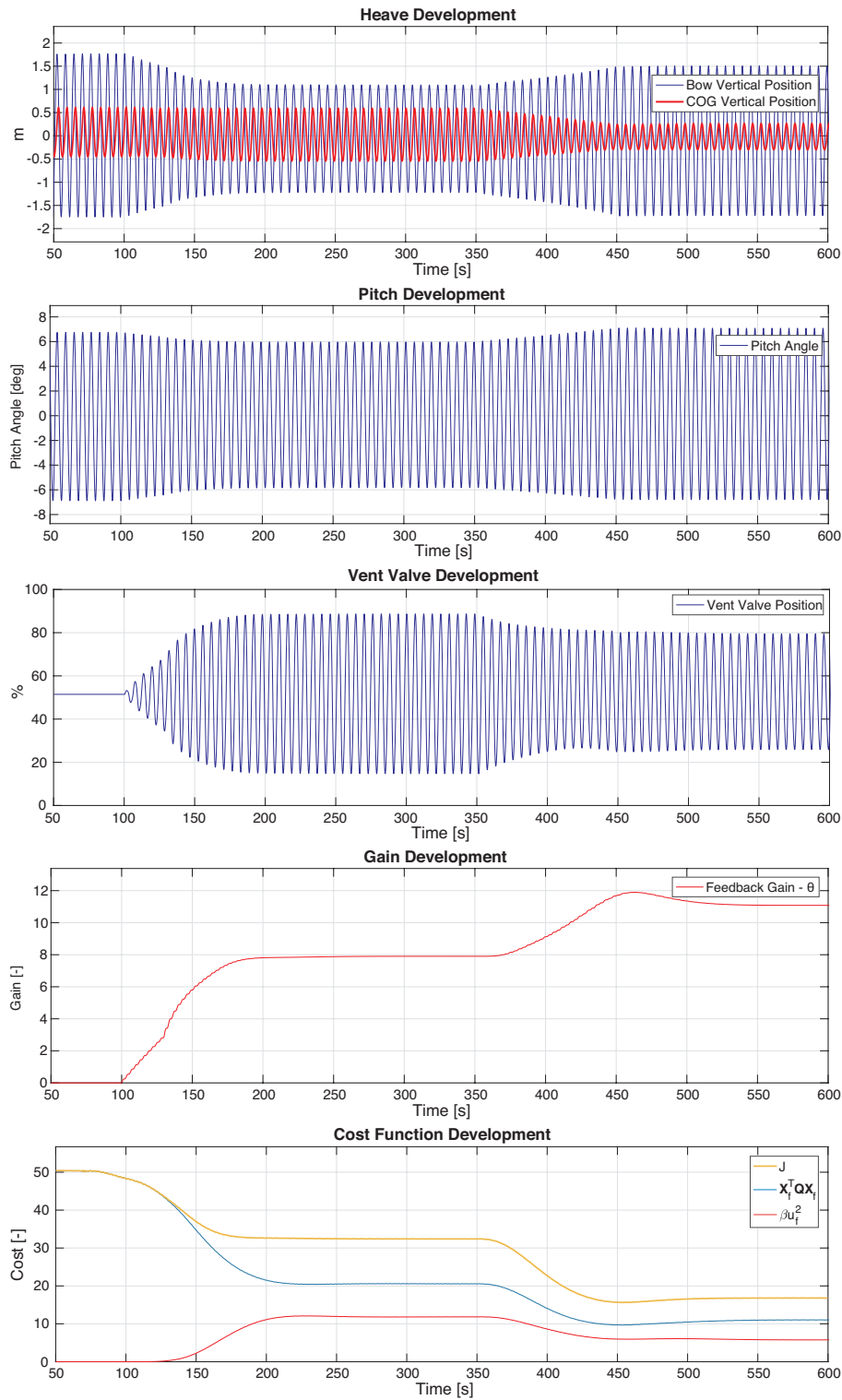


Figure 4.16: Simulation results for $H_s = 1.5 m$, $T_s = 6 s$ - Bow to COG Damping

In this simulation, control is applied at 100 s and damping is applied to the bow of the vessel. At 350 s the longitudinal point of where damping is injected is directed towards the COG and at 500 s the transition is complete with all damping being injected at the COG.

Compared to the previous case (Section 4.5.1) where damping is first injected at the COG, the initial response of the adaptive controller is similar. However, due to the higher velocities being observed at the bow, the feedback gain initially converges at a lower value. The vertical motion at the bow as well as the pitching motion is decreased, while the motion at the COG experience a slight increase. As the injected damping is directed towards the COG, both bow and pitching motions increase while the COG motions are reduced. Lower vertical motions recorded at the COG leads to a decrease in actuator usage, and the feedback gain is increased.

The results obtained here are comparable to the case with a decrease in sea state for regular waves (Section 4.2.2), where the adaptive scheme responds to the decrease in recorded motion and actuator usage by increasing the feedback gain.

4.6 Discussions

Overall the adaptive controller has shown capabilities of adjusting the controller parameters in a desirable manner. The controller is able to inject a sizeable amount of damping in all cases, with an acceptable degree of actuator usage. The adaptive scheme is defined as to search for a balance between the size of the vertical motions and actuator usage. The value of the feedback gain parameter of where this balance may be found, is altered by tuning of weighting matrices. For the results presented, these matrices have been tuned such that the system exhibits an acceptable ability of injecting damping, while restraining the actuators from spending too much time at their limits. This means that the developed adaptive scheme does not provide the gain parameter which introduces the maximum amount of damping, which is evident by how the results display that there is still available actuating power for the obtained gain parameters.

The main argument behind an adaptive approach to the presented control problem, is that if the gain is kept constant and the vessel motions increase, the actuator usage will increase as well. This may lead to the actuators jumping between their upper and lower limits, which would cause unnecessary wear on the actuators. In the opposite case, for calm seas and a gain parameter tuned for a higher degree of vessel motion, the usage of the actuators which should be close to zero, experience instabilities. This is due to how process noise on the measured feedback controller inputs is amplified, causing actuation of the vent valve louvers. This actuation induces vibrations, which in turn is picked up by the on-board accelerometers performing the measurements, and is again amplified causing increased vibrations in a positive feedback loop.

The developed controller is dependent on inputs of the slowly varying statistic of vessel motion and actuator usage. These measures are not easily obtained without excessive filtering which introduces delays on the input signals. The adaptive controller is in practice comparing the change in gain with a combination of change in vessel motion and actuator usage, and large delays on the inputs make it so that the controllers' ability to respond to these comparisons is limited. Signal filtering was applied with this in mind, to obtain a delay small enough for the controller to be able to respond to the changes in operating conditions, while providing a value of the feedback gain which did not fluctuate too much in the simulated conditions

The challenges faced by the chosen approach are evident when evaluating the results for irregular waves. Excessive tuning of the parameters of the adaptation scheme was required to obtain a functioning controller, in the range of simulation conditions. The dependence of the rate of change in value of the cost function is a large drawback of the proposed controller, as it is vulnerable to rapid changes in the inputs, which are naturally introduced by irregular waves, but could also come from wild points in the measurements or sensor noise.

The idea behind the approach was keeping the current feedback control law and abstracting the matter of finding a gain parameter, to a continuous optimization problem. The main challenge then became to tune the behavior of the adaptive controller, to address the implications of varying operating conditions. The described system contains a wide range of non-linear relations with regards to the vessel response for waves of different amplitudes and frequencies, and how control is applied through the vent valve louvers. These effects caused the introduction of a series of tuning and scaling parameters, required to obtain the desired controller outputs.

The environmental conditions applied in the simulations were chosen to resemble normal to high sea states of which the WAVECRAFT™ may encounter. A feasible set of tuning parameters was found for the range of simulations, and the adaptive controller yielded desirable results.

Chapter 5

Concluding remarks

5.1 Conclusion

A key feature of the WAVECRAFT™ Surface Effect Ship is its ability to counteract vertical wave induced vessel motions, by altering the air cushion pressure. The benefits of such a feature include increased accessibility to offshore wind farms and other offshore-based plants, where a boarding procedure may be compromised by heavy seas for conventional CTVs. This thesis has described an extension to the work of Auestad et al. (2015) on the Boarding Control System, where an adaptive approach has been taken to achieve autonomous adjustments controller parameters to obtain a desirable response in different operating conditions.

A manual provided by UMOE Mandal on how the feedback is tuned by the vessel operators on the full-scale vessel states that:

"Under normal circumstances, the gain value should be increased as long as the change provides further reduction in vertical accelerations and does not saturate the control outputs."

These guidelines are used as a basis for design and tuning of the developed adaptive controller, and results show that the adaptive controller is able to behave in coherence with how the manual tuning procedure is performed. The developed adaptive controller use the same set of actuators and measurements available on the full-scale vessel today, and is thus potentially applicable as an addition to the existing controller software.

Work on the thesis consisted of a study of the current mathematical models describing the SES

dynamics, which have been under continuous development for the past few decades. Insights from these studies are used in the implementation of a simplified control plant model, which incorporates the vessel dynamics relevant for the development of an adaptive controller. The developed controller is tested in a series of simulations representative of various operating conditions. The adaptive controller is also applied to the more complex process plant model (SES-Sim), to verify the controller performance in a model which includes dynamics that are omitted in the simplified model.

There are several limitations with regards to the applicability of the results obtained with the adaptive controller. The dependence on input signals of high quality, the time required for adaptation and the amount of introduced tuning parameters are some of the drawbacks of the presented approach. This is why other procedures of introducing adaptive control should be investigated.

However, simulations show that developed controller and adaptation scheme is able to exhibit desirable performance, in both regular and irregular waves, and for both bow and COG damping. This is obtained by calculating a feedback gain parameter, which provides a balanced amount of actuator usage and damping performance, without causing unnecessary actuator wear or introducing vibrations.

5.2 Further Work

The work described in this thesis indicates that an adaptive approach to the vertical motion control problem is feasible. However, the choice of developing an adaptive scheme as an extension of exciting feedback control law set restrictions to the development, yet an extension to the existing system has the advantage of being easily implementable. For further work on the presented adaptive controller, an alternative way of obtaining a measure of the degree vessel motion should be investigated, as this is one of the major weaknesses of the developed controller.

Comparing the draft of a SES in a fully off-cushion condition, to a vessel in fully *on-cushion* illustrates the capabilities of the SES to change its vertical position. Moreover, the use of vent valve louvers enables the cushion pressure to be altered rapidly at commonly encountered wave periods. Intuitively, it is suggested that there exists a control signal capable of near perfect cancellation of wave induced vertical motions, for the case where the magnitude of the induced motions are smaller than the SES ability to change its vertical position. The feedback control law presented in this thesis is vulnerable to delays in the measured inputs which is a limiting

factor in the ability to inject damping, even at smaller sea states. To obtain improved damping capabilities, research in alternative controller schemes is suggested.

The objective of this thesis was to develop an adaptive controller scheme, capable of providing a feedback gain parameter that renders acceptable performance in a range of operating conditions. For each simulation portrayed in the results of this thesis, the overall structure and parameters of the controller remain constant. Maintaining the same parameters and controller structure for such varying conditions has been a major challenge, and has been experienced to set limitations on the responsiveness of the controller. A *hybrid controller* setup with the potential of implementing more rapid changes to how control is executed in various operating conditions, is therefore suggested to be investigated as a more viable option.

Appendix A

Control Plant Model

A.1 Model Parameters

- $\rho_{c0} = 1.23 \frac{kg}{m^3}$
- $\rho_a = 1.23 \frac{kg}{m^3}$
- $\gamma = 1.4$
- $A_c = 160 m^2$
- $h_0 = 2 m$
- $p_0 = 200 mmWC$
- $c_n = 0.61$
- $L = 20 m$
- $x_{xp} = 0.5 m$
- $dQ = 69 \frac{m^3}{s}$
- $dp = -1410 mmWC$
- $Q_0 = 90 \frac{m^3}{s}$
- $d = 1.2 m$
- $m = 85000 kg$

- $I_{yy} = 4380000 \text{ kgm}^2$
- $A_{33} = 53300 \text{ kg}$
- $B_{33} = 4130 \frac{\text{kg}}{\text{s}}$
- $C_{33} = 35800 \frac{\text{N}}{\text{m}}$
- $A_{55} = 170000 \text{ kgm}^2$
- $B_{55} = 130000 \frac{\text{kgm}}{\text{s}^2}$
- $C_{55} = 11100000 \frac{\text{Nm}}{\text{rad}}$

$$\bullet \mathbf{A} = \begin{bmatrix} 0 & 0 & \frac{1}{m+A_{33}} & 0 & 0 \\ 0 & 0 & 0 & \frac{1}{I_{yy}+A_{55}} & 0 \\ -C_{33} & 0 & \frac{-B_{33}}{m+A_{33}} & 0 & A_c P_0 \\ 0 & -C_{55} & 0 & \frac{-B_{55}}{I_{yy}+A_{55}} & -x_{cp} A_c p_0 \\ 0 & 0 & \frac{\rho_{c0} A_c}{K_1(m+A_{33})} & \frac{x_{cp} \rho_{c0} A_c}{K_1(I_{yy}+A_{55})} & \frac{K_3}{K_1} \end{bmatrix}$$

$$\bullet \mathbf{B} = \begin{bmatrix} 0 \\ 0 \\ 0 \\ 0 \\ \frac{K_2}{K_1} \end{bmatrix}$$

A.2 Controller parameters

- $k = 0.2$
- $k_j = 0.1$
- $\mathbf{C} = \begin{bmatrix} 0 & 0 & \frac{k_b+k_c}{m+A_{33}} & \frac{-k_c x_{cl} b}{I_{55}+A_{55}} & 0 \end{bmatrix}$
- $\mathbf{Q} = \begin{bmatrix} 0 & 0 & 350k_c & 5k_b & 0 \end{bmatrix}$
- $\omega_f = 0.03 \frac{\text{rad}}{\text{s}}$

Appendix B

Additional results

B.1 CPM - Initialization and Transition from H_s 0.8 to 1.4 m - Regular Waves

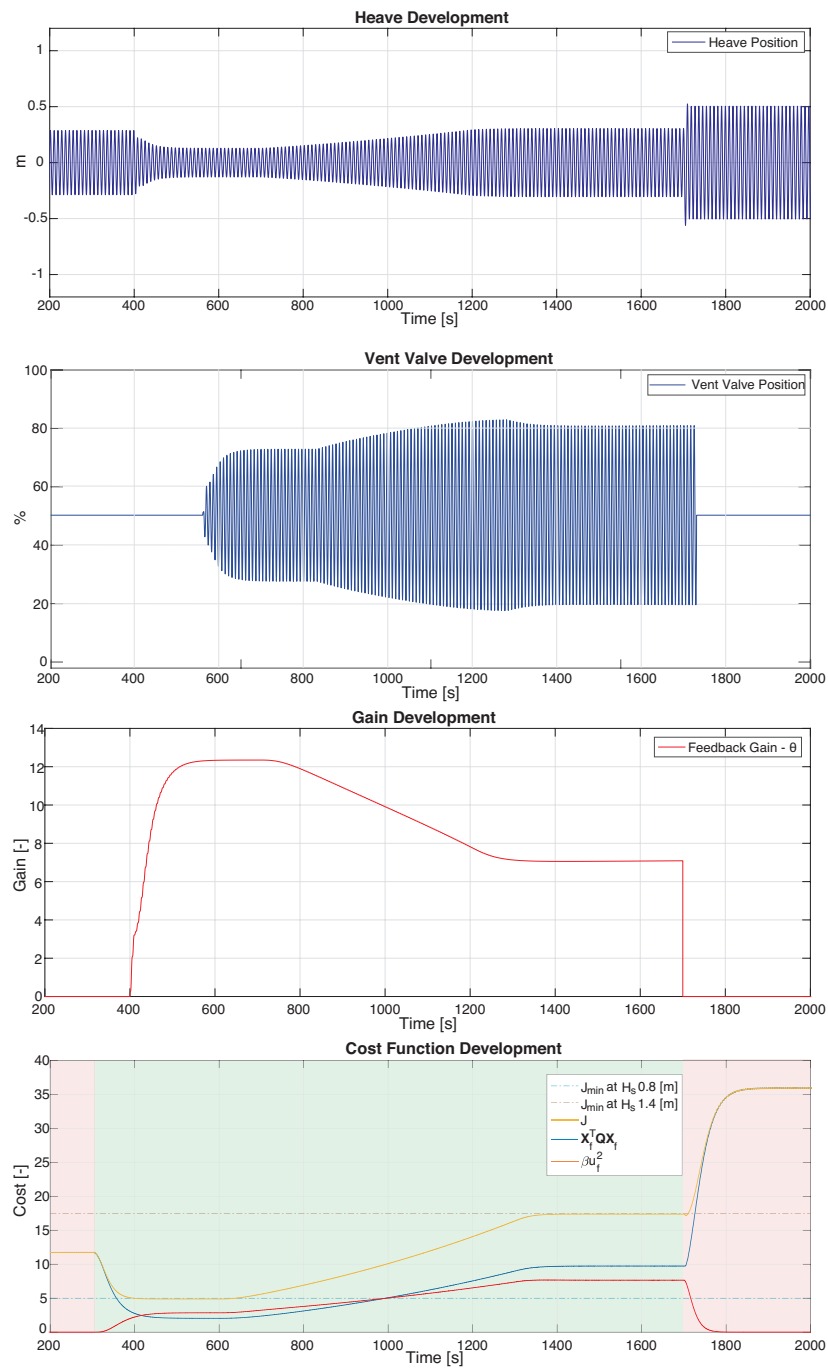


Figure B.1: Simulation results for $H_s = 1.4$ m, $T_s = 7.5$ s to $H_s = 2$ m, $T_s = 8.8$ s

B.2 CPM - Initialization and Transition from H_s 1.4 to 0.8 m - Regular Waves

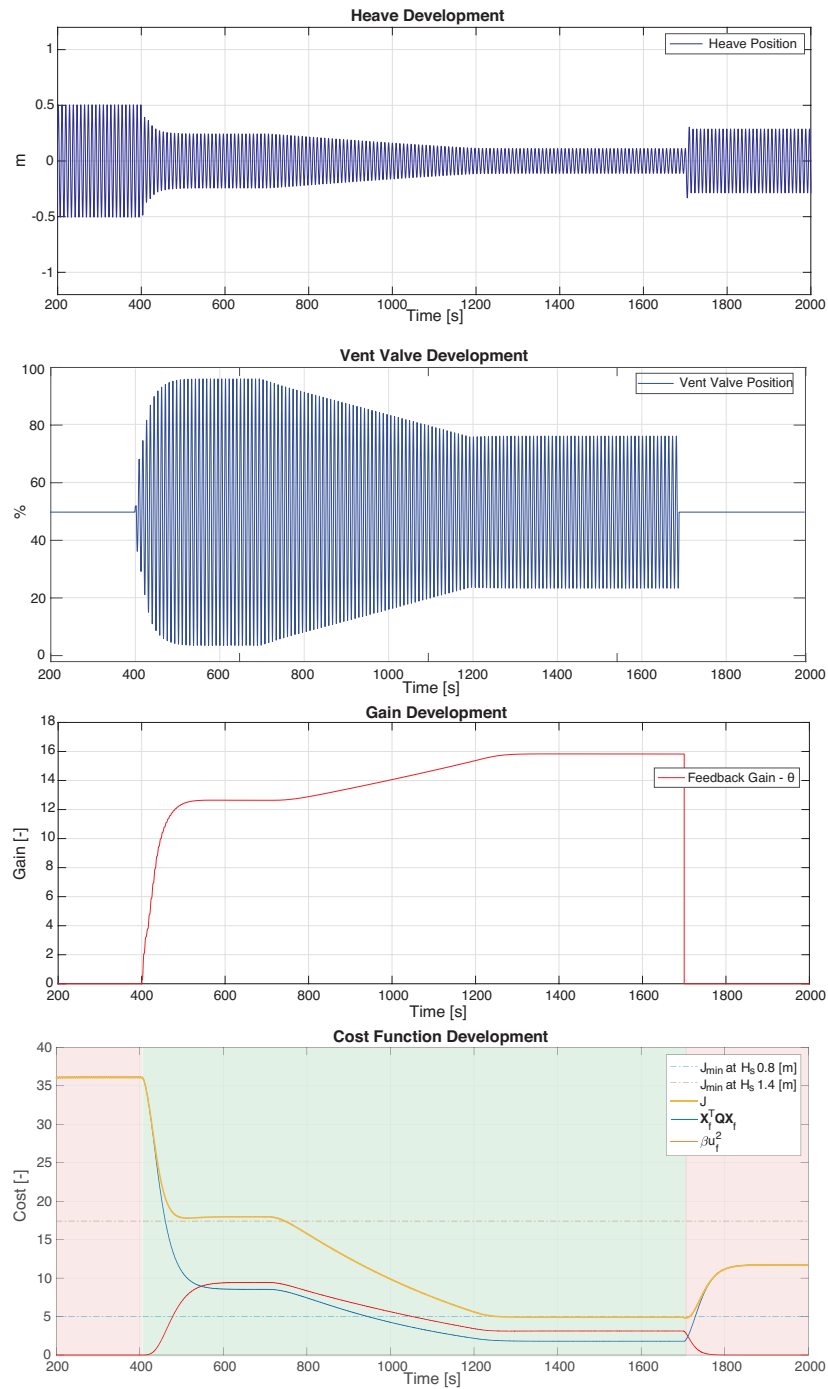


Figure B.2: Simulation results for $H_s = 1.4$ m, $T_s = 7.5$ s to $H_s = 2$ m, $T_s = 8.8$ s

Appendix C

List of Attached Files

- **conferenceposter.pdf** - A conference poster created for a poster exhibition at NTNU presenting the work on SES by students Kai Chen and Snorre Fjellvang.
- **processplant.slx** - A *Simulink* model with the implemented control plant model.
- **definevariables.m** A Matlab-script defining the necessary variables to run the Simulink model.

Bibliography

- Adams, J. D., Ernest, A. W., and Lewis, J. (1983). Design, Development and Testing of a Ride Control System for the XR-ID Surface Effect Ship;. *Technical Report*.
- Auestad, Ø. F., Gravdahl, J. T., and Fossen, T. I. (2013a). *Heave motion estimation on a craft using a strapdown inertial measurement unit*, volume 9. IFAC.
- Auestad, Ø. F., Gravdahl, J. T., Perez, T., Sørensen, A. J., and Espeland, T. H. (2015). Boarding control system for improved accessibility to offshore wind turbines: Full-scale testing. *Control Engineering Practice*, 45:207–218.
- Auestad, Ø. F., Gravdahl, J. T., Sørensen, A. J., and Espeland, T. H. (2013b). Simulator and control system design for a free floating surface effect ship at zero vessel speed. *IFAC Proceedings Volumes (IFAC-PapersOnline)*, 8(PART 1):67–72.
- Basturk, H. (2013). Disturbance Cancellation by State Derivative Feedback with Application to Ramp-Connected Surface Effect Ships. Technical report.
- Butler, E. A. (1985). the Surface Effect Ship. *Naval Engineers Journal*, 97(2):200–253.
- Cummins, W. E. (1962). *The Impulse Response Function and Ship Motions*.
- Det Norske Veritas (2011). Modelling and Analysis of Marine Operations. Technical report.
- Faltinsen, O. M. (1990). *Sea Loads on Ships and Offshore Structures*. Cambridge.
- Faltinsen, O. M. (2005). *Hydrodynamics of High Speed Marine Vehicles*. Cambridge.
- Fathi, D. and Hoff, J. R. (2004). *SipX Vessel Responses (VERES) - Theory Manual*.
- Fossen, T. I. (2011). *Handbook of Marine Craft Hydrodynamics and Motion Control*. Wiley.
- Fossen, T. I. and Smogeli, Ø. N. (2004). Nonlinear Time-Domain Strip Theory Formulation for Low-Speed Manoeuvring and Station-Keeping. *Modeling, Identification and Control*, 25(4):201–221.

- Kaplan, P., Bentson, J., and Davis, S. (1981). Dynamics and Hydrodynamics of Surface-Effect Ships. *SNAME Transactions*, 89:211–247.
- Kaplan, P. and Davis, S. (1974). A simplified representation of the vertical plane dynamics of the SES craft. Technical report.
- Kristiansen, E. and Egeland, O. (2013). Frequency-Dependent Added Mass in Models for Controller Design for Wave Motion Damping. *IFAC Proceedings Volumes (IFAC-PapersOnline)*, 36(21):67–72.
- Küchler, S., Eberharter, J. K., Langer, K., Schneider, K., and Sawodny, O. (2011). Heave motion estimation of a vessel using acceleration measurements. *IFAC Proceedings Volumes (IFAC-PapersOnline)*, 18(PART 1):14742–14747.
- Moran, D. D. (1975). The Wave Height under a High Length-to-Beam Ratio Surface-Effect-Ship in Regular Waves. *Ship Performance Department - U.S Navy*.
- Moran, D. D. (1976). Cushion Pressure Influences on a High Length-To-Beam Ratio Surface Effect Ship in Irregular waves. *Ship Performance Department - U.S Navy*.
- Perez, T., Fossen, T. I., and Sørensen, A. J. (2004). A Discussion About Seakeeping and Manoeuvring Models For Surface Vessels. Technical report, Centre for Ships and Ocean Structures (CESOS) Norwegian University of Science and Technology NTNU, Trondheim, Norway.
- Perez, T., Smogeli, Ø. N., Fossen, T. I., and Sørensen, A. J. (2006). An overview of the marine systems simulator (MSS): A simulink® toolbox for marine control systems. *Modeling, Identification and Control*, 27(4):259–275.
- Sørensen, A. J. (2013). *Marine Control Systems: Propulsion and Motion Control of Ships and Ocean Structures*. Department of Marine Technology NTNU.
- Sørensen, A. J. and Egeland, O. (1995). Design of ride control system for surface effect ships using dissipative control. *Automatica*, 31(2):183–199.
- Sørensen, A. J., Steen, S., and Faltinsen, O. M. (1993). SES Dynamics in the Vertical Plane. *Ship Technology Research*, 40:71–94.
- Steen, S. (1993). *Cobblestone effect on SES*. PhD thesis, NTNU, Trondheim, Norway.
- Ulstein, T. (1995). *Nonlinear effects of a flexible stern seal bag on cobblestone oscillations of an SES*. PhD thesis, NTNU, Trondheim, NORWAY.

windeurope (2017). Offshore wind in Europe: Key Trends and Statistics. <https://windeurope.org/about-wind/statistics/offshore/european-offshore-wind-industry-key-trends-statistics-2017/>.